in silico Plants
OXFORD UNIVERSITY PRESS

Original Research

HydroShoot: a functional-structural plant model for simulating hydraulic structure, gas and energy exchange dynamics of complex plant canopies under water deficit—application to grapevine (*Vitis vinifera*)

R. Albasha[1,2], C. Fournier[1], C. Pradal[3,4,5], M. Chelle[6], J. A. Prieto[7], G. Louarn[8], T. Simonneau*[1] and E. Lebon†[1]

[1]INRA, UMR759 LEPSE, F-34060 Montpellier, France
[2]itk, Clapiers, France
[3]CIRAD, UMR AGAP, Montpellier, France
[4]AGAP, Univ. Montpellier, CIRAD, INRA, Montpellier SupAgro, Montpellier, France
[5]INRIA, Univ. Montpellier, Montpellier, France
[6]INRA, UMR1402 Ecosys, F-78850 Thiverval-Grignon, France
[7]INTA EEA Mendoza, San Martín 3853, Luján de Cuyo 5507, Mendoza, Argentina
[8]INRA, UR4 P3F, Route de Saintes, BP 6, F-86600 Lusignan, France

Received: 27 February 2019 **Editorial decision:** 20 May 2019 **Accepted:** 29 May 2019

Citation: Albasha R, Fournier C, Pradal C, Chelle M, Prieto JA, Louarn G, Simonneau T, Lebon E. 2019. HydroShoot: a functional-structural plant model for simulating hydraulic structure, gas and energy exchange dynamics of complex plant canopies under water deficit—application to grapevine (*Vitis vinifera*). *In Silico Plants* **2019**: diz007; doi: 10.1093/insilicoplants/diz007

Abstract. This paper presents HydroShoot, a leaf-based functional-structural plant model (FSPM) that simulates gas exchange rates of complex plant canopies under water deficit conditions. HydroShoot is built assuming that simulating both the hydraulic structure of the shoot together with the energy budget of individual leaves is the asset for successfully scaling-up leaf to canopy gas exchange rates. HydroShoot includes three interacting modules: *hydraulic*, which calculates the distribution of xylem water potential across shoot hydraulic segments; *energy*, which calculates the complete energy budget of individual leaves; and *exchange*, which calculates net carbon assimilation and transpiration rates of individual leaves. HydroShoot was evaluated on virtual and real grapevines having strongly contrasted canopies, under well-watered and water deficit conditions. It captured accurately the impact of canopy architecture and soil water status on plant-scale gas exchange rates and leaf-scale temperature and water potential. Both shoot hydraulic structure and leaf energy budget simulations were, as postulated, required to adequately scaling-up leaf to canopy gas exchange rates. Notwithstanding, simulating shoot hydraulic structure was found more necessary to adequately performing this scaling task than simulating leaf energy budget. That is, the intra-canopy variability of leaf water potential was a better predictor of the reduction of whole plant gas exchange rates under water deficit than the intra-canopy variability of leaf temperature. We conclude that simulating the shoot hydraulic structure is a prerequisite if FSPMs are to be used to assess gas exchange rates of complex plant canopies as those of grapevines. Finally, HydroShoot is available through the OpenAlea platform (https://github.com/openalea/hydroshoot) as a set of reusable modules.

[†]In memory of Eric Lebon

* Corresponding author's e-mail address: thierry.simonneau@inra.fr

© The Author(s) 2019. Published by Oxford University Press on behalf of the Annals of Botany Company.
This is an Open Access article distributed under the terms of the Creative Commons Attribution License (http://creativecommons.org/licenses/by/4.0/), which permits unrestricted reuse, distribution, and reproduction in any medium, provided the original work is properly cited.

Keywords: Energy budget; functional-structural plant model (FSPM); gas exchange; grapevine (*Vitis vinifera*); hydraulic structure; water deficit.

Introduction

Climate change is seriously challenging viticulture sustainability in its current areas of production (Hannah *et al.* 2013; Duchêne *et al.* 2014; van Leeuwen and Philippe 2016). One efficient short-term solution for hampering the projected adverse effects of water and heat stress on viticulture is to reconsider training systems so that they allow maximizing the ratio of carbon assimilation ($A_{n,plant}$) to water loss by transpiration (E_{plant}) while maintaining optimal leaf temperature conditions (Medrano *et al.* 2012; Duchêne *et al.* 2014; Palliotti *et al.* 2014). However, training systems present a wealth of possibilities (Reynolds and Vanden Heuvel 2009) that cannot be compared experimentally. Therefore, the design of canopy structures that are adapted to adverse environmental conditions is most efficiently performed with the aid of models able to accurately predict the influence of canopy architecture on its gas exchange rates and leaves temperature under combined water and heat stress. That is what functional-structural plant models (FSPMs) offer (Vos *et al.* 2010).

FSPMs received nevertheless little attention in grapevine scientific literature to assess the impact of shoot architecture on plant gas exchange rates (Medrano *et al.* 2015a). This is probably due to the inherent complexity in scaling-up eco-physiological processes from the leaf to the canopy level, as strong variability in gas exchange rates (CO_2 versus water vapour) exists inside the canopy driven by variations in micrometeorological conditions and leaf functional traits (Medrano *et al.* 2015b; Niinemets *et al.* 2015). This scaling-up task is even more complex under water deficit conditions, as stomatal aperture is likely to reduce under water deficit in a non-uniform pattern across the canopy (e.g. Gonzalez-Dugo *et al.* 2012; Ngao *et al.* 2017) further distorting intra-canopy gas exchange and leaf temperature variability (Reynolds and Vanden Heuvel 2009). Bauerle *et al.* (2007) indicated that disregarding this variability may lead to strongly overestimate the predicted whole canopy daily transpiration flux, up to 25 % greater than observed values as they found on a study on red maple (*Acer rubrum*)

Hence, adequately predicting the intra-canopy variability of both leaf stomatal conductance and temperature stands out as the key challenge to using FSPMs to predict plant gas exchange rates under water deficit conditions. Yet, the remaining question is how this variability can be accurately described and what are their main determinants.

Describing the intra-canopy variability of both leaf stomatal conductance and temperature requires from the one hand to explicitly describe their drivers as a function of leaf position inside the canopy, and from the other hand to adequately account for their mutual interactions (how stomatal aperture affects leaf energy budget and *vice versa*) (Chelle 2005). The main drivers for both processes are commonly determined as incident shortwave irradiance, air temperature, air humidity and leaf 'water status' which determines stomatal closure (Damour *et al.* 2010). Among these drivers, leaf water status (which controls stomatal aperture and consequently both leaf transpiration and temperature) still makes no consensus in the scientific literature when it comes to determining what it refers to. A basal approach considers that leaf water status is equal to the soil water status (e.g. van Wijk *et al.* 2000; Misson *et al.* 2004), considering that the 'remote' action of available water in the rhizosphere impacts uniformly all leaves regardless of their position. By contrast, leaf water status may also be considered as a 'local' water status specific to each individual leaf (e.g. Buckley *et al.* 2003; Tuzet *et al.* 2003) which results from the interplay between water demand (transpiration) and offer (xylem flow) at the leaf scale, which are notably determined by the shoot hydraulic structure. This 'local' approach mostly agrees with observations whereby stomatal closure is uneven across the canopy. Sunlit leaves, for instance, experience stronger water deficit than shaded leaves, and are therefore the first to undergo reductions in gas exchange rates under water deficit (Escalona *et al.* 2003). This 'local' approach seems hence as the most adequate in FSPMs; however, the 'remote' modelling approaches also proved satisfactory when individually considered (e.g. Dauzat *et al.* 2001; Bailey *et al.* 2016; Ngao *et al.* 2017). It is hence unclear in literature how the simulation of leaf water status of individual leaves affects the predicted gas exchange rates and leaf temperature distribution in FSPMs under water deficit and this matter needs to be assessed if FSPMs are to be used under water deficit conditions.

The few existing grapevine FSPMs in literature do not account for the interactions between water status, energy budget and gas exchange rates at the leaf scale **[see Supporting Information S1]**. Prieto *et al.* (2012) were probably the first to use an FSPM to examine the effects of canopy architecture on gas exchange in grapevine (cv. Syrah). The authors coupled the grapevine-specific structural plant model proposed by Louarn *et al.* (2008) to leaf-level models of photosynthesis (Farquhar *et al.* 1980) and stomatal conductance (Leuning 1995) but did not incorporate the effects of (soil) water deficit. More recently, Zhu *et al.* (2018) developed a model similar to that proposed by Prieto *et al.* (2012) including the effect of water deficit on gas exchange and leaf temperature. Nevertheless, this model assumed a uniform xylem water potential across the shoot, that disregarded how shoot hydraulic structure affects leaf-scale gas exchange rates, which is an unrealistic assumption for large plants when considering the substantial hydraulic resistances observed in the stems of mature grapevine (Jacobsen and Pratt 2012). In addition, longwave energy exchange among leaves from the one hand, and between leaves and the surrounding elements from the other hand, were disregarded, which makes the application of this model to open field conditions not suitable since sky and soil longwave energies substantially affect leaves temperature (Nobel 2005). This has been solved in two models that link a complete energy budget with gas exchange in perennials (Bailey *et al.* 2016 for *Vitis vinifera* and *Acer* × *freemanii*; Ngao *et al.* 2017 for *Malus pumila*). Yet again, both models were built at the leaf-cluster scale which does not allow accounting for the location of individual leaves in plant hydraulic structure necessary to calculate local leaf water status. In addition, both models consider the 'remote' action of the rhizosphere on stomatal aperture instead of the 'local' water status, assuming again as negligible the potential contribution of shoot hydraulic structure on shaping the intra-canopy variability of leaf stomatal conductance and temperature.

In this paper, it is postulated that intra-canopy variability in both leaf water potential and leaf temperature are the main drivers for adequately predicting photosynthesis and transpiration fluxes at the plant scale under water deficit conditions using FSPMs. This paper has 3-fold objective. The first is to describe HydroShoot, a leaf-scale-based FSPM that allows predicting whole plant transpiration and photosynthesis rates by scaling-up these processes from the leaf-level. This model uses as lever for this scaling process the simulation of the interactions between hydraulic structure of the shoot, the energy balance and gas exchange rates of individual leaves. The second objective is to evaluate the performance of the model using both virtual and real canopies with data collected on photosynthesis and transpiration rates (plant scale), and stomatal conductance and temperature (leaf scale). Finally, the third objective is to examine how detailed hydraulic structure and energy budget simulations determine the predicted gas exchange rates at the plant scale under water deficit conditions.

Materials and Methods

Model structure and basic assumptions

HydroShoot is a static FSPM (with regards to plant structure) that takes plant shoot architecture, weather and soil water conditions as inputs, and returns transpiration and net photosynthesis rates both of individual leaves and the whole plant at hourly time steps as outputs. It is conceived as a set of three modules which simulate water potential (*hydraulic* module), energy budget (*energy* module) and C_3-type gas exchange rates (*exchange* module). These three modules run jointly, having leaf xylem water potential and temperature at the leaf-level as pivots (cf. Implementation and numerical resolution section). The formalisms used in each module are developed in the following sections.

Hydraulic module. The *hydraulic* module computes water potentials of plant segments (output of the module) as a function of water flow in the plant and water potential of the soil (input to the module). The whole plant is compartmentalized in elementary conducting elements corresponding to petioles, internodes of the current-year stems and elements of previous-year trunk and branches (internodes or pruning complexes). Leaves are treated in this system as nodes letting water flow but having no gradient in their water potential (Ψ_{leaf}).

Water transfer across the hydraulic segments is simulated by analogy to Ohm's law in electrical circuits (Fig. 1). Each segment is characterized by its length (L, m) and hydraulic conductivity (K, kg s^{-1} m MPa^{-1}), and is crossed by a water flux (F, kg s^{-1}) which, together with conductivity, modifies water head at its upper (downstream, H_u) and lower (upstream, H_l) extremities [MPa]:

$$F_i = -K_i \frac{H_{u,i} - H_{l,i}}{L_i} = -K_i \frac{\Psi_{u,i} - \Psi_{l,i} + \rho g \left(z_{u,i} - z_{l,i}\right)}{L_i} \quad (1)$$

where i denotes the segment identifier, $\Psi_{u,i}$ and $\Psi_{l,i}$ are, respectively, xylem water potential at the upper and lower extremities, $z_{u,i}$ and $z_{l,i}$ are elevations of upper and lower extremities [m], respectively, ρ is water density [kg m^{-3}] and g is the gravitational acceleration [m s^{-2}].

Xylem conductivity varies with water potential as a result of xylem cavitation under water deficit (Tyree and Sperry 1989). This relationship is described using a sigmoidal function:

$$K_i = K_{max,i} \frac{1}{1 + \left(\frac{\Psi_i}{\Psi_{icrit,stem}}\right)^{c_{x1}}} \quad (2)$$

where $K_{max,i}$ is the maximum segment conductivity [kg s^{-1} m MPa^{-1}], Ψ_i is the arithmetic mean of water potential values of the segment i $\left(\frac{\Psi_{u,i}+\Psi_{l,i}}{2}\right)$, $\Psi_{icrit,stem}$ [MPa] and

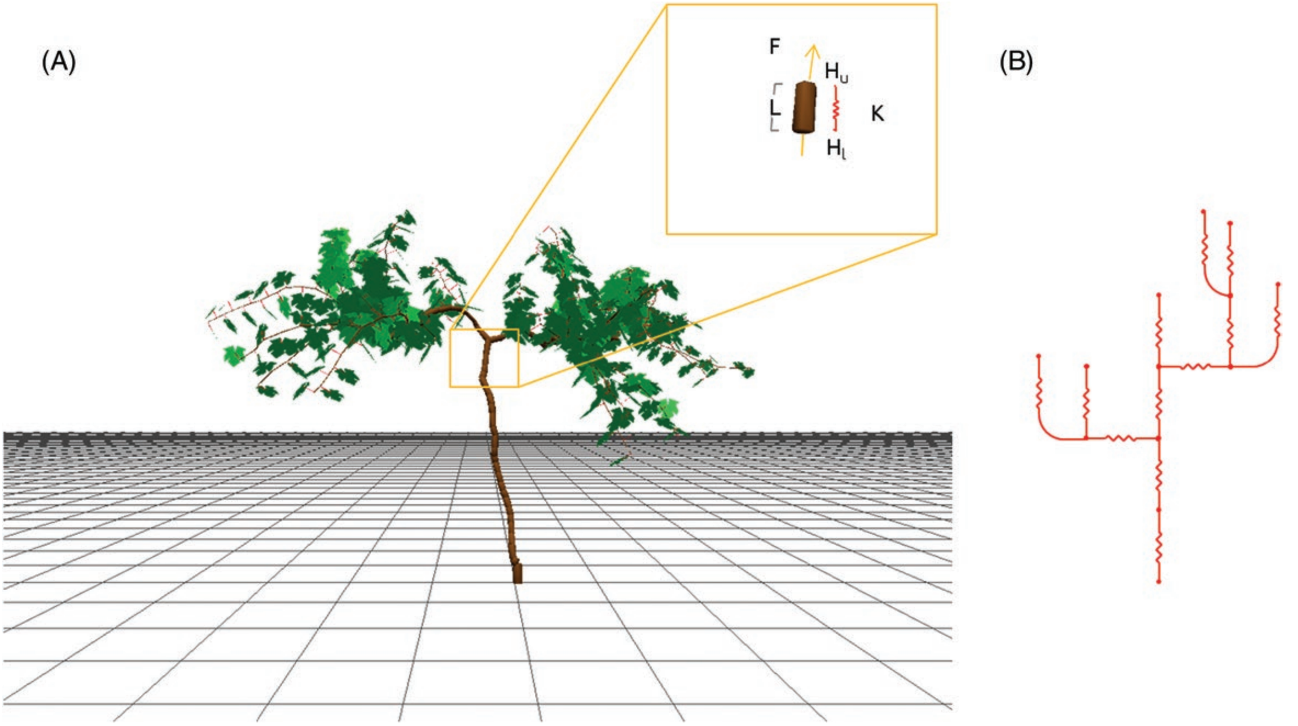

Figure 1. (A) Illustration of the parameters required to calculate the hydraulic structure: *F*, rate of water flow [kg s^{-1}]; *K*, hydraulic conductivity per unit length of the hydraulic segment [kg s^{-1} m MPa^{-1}]; *L*, length of the hydraulic segment [m]; and H_u and H_l are, respectively, water potentials at upper (downstream) and lower (upstream) extremities of the hydraulic segment [MPa]. (B) The schematic representation of the electrical analog.

c_{x1} [–] are shape parameters. $K_{max,i}$ is estimated empirically as proposed by Tyree and Zimmermann (2002):

$$K_{max,i} = c_{x2}\ D_i^{c_{x3}} \tag{3}$$

where D_i is segment average diameter [m] and c_{x2} and c_{x3} are dimensionless shape parameters, mostly given within the ranges of [2.5, 2.8] and [2.0, 5.0], respectively (Tyree and Zimmermann 2002).

Equations (1–3) apply to all conducting segments (not leaves blades). Water potential of the upper extremity of the petiole is assumed equal to that of the lumped leaf water potential Ψ_{leaf}.

Exchange module. The *exchange* module computes the rates of net carbon assimilation and transpiration per unit surface area (A_n and *E*, respectively) for each individual leaf as a function of micrometeorological conditions and leaf water status. The calculations use the analytical solution proposed by Yin and Struik (2009) for coupling the C_3 photosynthesis model of Farquhar *et al.* (1980) to the stomatal conductance model of Ball *et al.* (1987). This coupling allows stomatal conductance (to both CO$_2$ and water vapour) to respond to environmental stimuli (temperature and irradiance) via photosynthesis **[see Supporting Information S2]**. It is based on Fick's first law of diffusion, whereby A_n, the stomatal conductance to CO$_2$ (g_{s,CO_2}), and the mesophyll conductance (g_m) are used. However, as Farquhar's model has been thoroughly detailed in literature, its description is given in Appendix 1. The focus of this section is given instead to the stomatal conductance formulae which are a key element in this work.

$A_{n,plant}$ is calculated according to Yin and Struik (2009) as:

$$g_{s,CO_2} = g_{s0,CO_2} + m_0 \frac{A_n + R_d}{(C_i - \Gamma)} f_w \tag{4}$$

where g_{s0,CO_2} is the residual stomatal conductance to CO$_2$ $mol\,m^{-2}s^{-1}$, R_d is mitochondrial respiration in the light [$\mu mol\,m^{-2}s^{-1}$], C$_i$ is intercellular CO$_2$ concentration µmol mol^{-1} Γ is CO$_2$ compensation point in the absence of mitochondrial respiration [$\mu mol\,mol^{-1}$], m_0 is a dimensionless shape parameter and f_w is a dimensionless function representing the response of g_{s0,CO_2} to air water vapour deficit (VPD, kPa). f_w is deduced from the stomatal conductance model of Leuning (1995) as:

$$f_w = \frac{1}{\left(1 + \frac{VPD}{D_0}\right)} \tag{5a}$$

where D_0 is a scaling parameter [kPa].

Equation (5a) does not account for stomatal sensitivity to soil water deficit ('remote' approach) or local leaf water potential ('local' approach). Tuzet *et al.* (2003) and Leuning *et al.* (2004) suggested to express f_w as a function of the local Ψ_{leaf}. This function is implemented in HydroShoot following Nikolov *et al.* (1995):

$$f_w = \frac{1}{1 + \left(\frac{\Psi_{leaf}}{\Psi_{crit,leaf}}\right)^n} \tag{5b}$$

where $\Psi_{crit,leaf}$ is a critical leaf water potential threshold [MPa] at which stomatal conductance is reduced by 50%, and n is a shape parameter [–]. The same last equation is used to express the dependency of RMSE on the remote soil water potential (Ψ_{soil}):

$$f_w = \frac{1}{1 + \left(\frac{\Psi_{soil}}{\Psi_{crit,leaf}}\right)^n} \tag{5c}$$

The transpiration rate $E\left[\mathrm{mol_{H_2O}\ m^{-2}\ s^{-1}}\right]$ is calculated as:

$$E = \frac{1}{\frac{1}{g_{b,H_2O}} + \frac{1}{1.6\ g_{s,CO_2}}} \left(\frac{\mathrm{VPD}}{P_a}\right) \tag{6}$$

where P_a is the atmospheric pressure [MPa] and g_{b,H_2o} is the boundary layer conductance to water vapour $\left[\mathrm{mol_{H_2o}\ m^{-2} s^{-1}}\right]$, derived from Nobel (2005) as:

$$g_{b,H_2O} = \frac{D_{H_2O} * P_v}{R\ T\ \Delta x} \tag{7}$$

with

$$D_{H_2O}\,(t) = D_{H_2O} \frac{P_a}{P_v} \left(\frac{T}{273}\right)^{1.8} \tag{8}$$

where D_{H_2o} is the diffusion coefficient of H_2O in the air at 0 °C (2.13*10^{-5} m^2 s^{-1}), P_a is the ambient air pressure at 0 °C temperature [MPa], P_v is water vapour partial pressure [MPa] and Δ*x* is the thickness of the boundary layer [m] which is defined as (Nobel 2005):

$$\Delta x = 0.004 \sqrt{\frac{l}{v}} \tag{9}$$

where *l* is the mean length of the leaf in the downwind direction [m], set to 70% of blade length, and *v* is the ambient wind speed [m s^{-1}].

Finally, mesophyll conductance to CO_2 is assumed to simply depend on bulk leaf temperature (Evers *et al.* 2010) following an Arrhenius equation trend (as for photosynthetic parameters, cf. equation (A8)) with a basal value at 25 °C set to 0.1025 $\left[\mathrm{mol\ m^{-2} s^{-1}}\right]$.

Intra-canopy variability in photosynthetic capacity. Leaf photosynthetic traits (maximum carboxylation rate V_{cmax}, maximum electron transport rate J_{max}, triose phosphate transport rate TPU and R_d; cf. Appendix 1) have been shown to strongly vary within the plant canopy so that to increase light-saturated net assimilation rate with increasing solar irradiance availability throughout the canopy (Niinemets *et al.* 2015). HydroShoot accounts for this variability by considering leaf nitrogen content per unit leaf surface area (N_a, g_N m^{-2}) as the pivotal trait to determine the photosynthetic capacity of leaves (Prieto *et al.* 2012) as follows:

$$P^{25} = S_{N_a} N_a - b_{N_a} \tag{10}$$

where P^{25} is the value at 25 °C for any of the rates V_{cmax}, J_{max}, TPU and R_d (given as inputs), and $S_{N_a}\left[\mathrm{\mu mol_{CO_2}\quad g_N{}^{-1}\ s^{-1}}\right]$ and $b_{N_a}\left[\mathrm{\mu mol_{CO_2}\quad m^{-2}\ s^{-1}}\right]$ are the slope and the intercept of the linear relationship with N_a specific to each rate. N_a is calculated as the product of nitrogen content per unit leaf dry mass N_m [g_N $g_{drymatter}{}^{-1}$] and leaf dry mass per area LMA [$g_{drymatter}$ m^{-2}]. N_m linearly varies with plant age, expressed as the thermal time cumulated from budburst (input of the model), and LMA is determined by leaf exposure to light during the last past days (Prieto *et al.* 2012). This is expressed respectively in the two following equations:

$$N_m = a_N \sum_{i=budburst}^{d} \left(max\left(0, T_{air,i} - T_b\right)\right) + b_N \tag{11}$$

$$\mathrm{LMA} = a_M ln\left(\mathrm{PPFD}_{10}\right) + b_M \tag{12}$$

where $T_{air,i}$ is the mean temperature of the day *i* [°C] and T_b is the base temperature (minimum required for growth) [°C], set to 10 °C for grapevine and used for the calculation of thermal time since budburst, a_N $\left[\mathrm{g_N\quad g_{drymatter}{}^{-1}\ {}^{\circ}Cd^{-1}}\right]$ and b_N $\left[\mathrm{g_N\quad g_{drymatter}{}^{-1}}\right]$ are the slope and intercept of the linear relationship between N_m and accumulated thermal time since budburst, PPFD_{10} [$\mathrm{mol_{photon}}$ m^{-2} d^{-1}] is the cumulative photosynthetic photon flux density irradiance intercepted by the leaf (output of the energy module) averaged over the past 10 days, and a_M $\left[\mathrm{g_{drymatter}\ \ mol_{photon}{}^{-1d}}\right]$ and b_M $\left[\mathrm{g_{drymatter}\quad m^{-2}}\right]$ are the slope and intercept of the linear relationship between LMA and the logarithm of PPFD_{10}.

Finally, this module was provided with a photoinhibition model as this phenomenon is frequently reported to affect grapevines under combined heat and water stresses (Correia *et al.* 1990; Flexas and Medrano 2002; Lovisolo *et al.* 2010). The simple photoinhibition model implemented in HydroShoot is detailed in Appendix 2 and assumes that combined heat and water stresses inhibit photosynthesis by reducing the electron transport rate (cf. *J* in equation (A6)) as the result of an increase of deactivation energy ΔH_d (cf. equations (A9) and (A10)).

Energy module. The *energy* module computes the temperature of individual leaves based on a detailed energy balance model (Gutschick, 2016) **[see Supporting Information S3]**. This module will be briefly described hereafter for the sake of simplicity.

Each leaf is represented as a group of solid flat triangles. It gains energy from the absorbed shortwave (solar irradiance) and thermal longwave irradiance from the sky, the soil and the neighbouring leaves (indexed *j*). It loses energy through its own emission in the thermal longwave band and through latent heat due to transpiration (output of *exchange* module). Finally, it exchanges energy with the surrounding air by thermal conduction–convection. The resulting leaf-scale energy balance equation writes:

$$\begin{aligned}0 &= \alpha_{i,R_g}\Phi_{iR_g}\\ &+\varepsilon_{i,leaf}\sigma\left(k_{i,sky}\varepsilon_{sky}T^4_{sky}+k_{i,soil}\varepsilon_{soil}T^4_{soil}+\sum_{j\in\Omega}T^4_jF_{ij}\right)\\ &-2\varepsilon_{i,leaf}\sigma T^4_i-\lambda E_i-2K_{air}\frac{(T_i-T_{air})}{\Delta x_i}\end{aligned} \quad (13)$$

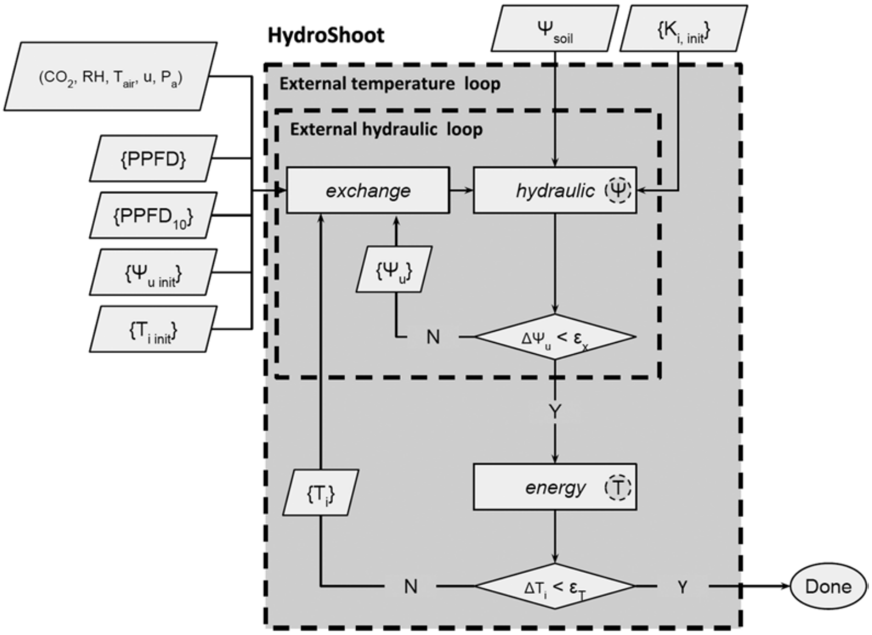

Figure 2. Schematic representation of the numerical resolution of HydroShoot. Meteorological inputs that are common to all leaves are air temperature (T_{air}, K), air relative humidity (RH, –), air CO$_2$ concentration [µmol mol^{-1}], wind speed (*u*, m s^{-1}) and atmospheric pressure (P_a, kPa). Inputs per individual leaves are the absorbed photosynthetic photon flux density (PPFD, µmol m^{-2} s^{-1}) and PPFD$_{10}$, the absorbed PPFD during the last 10 days. Ψ_u is xylem water potential at the nodes between each pair of hydraulic segments [MPa]. $\Psi_{u,init}$ is initial Ψ_u [MPa]. Ψ_{soil} is soil water potential. T_i is leaf temperature [K]. $T_{i,init}$ is initial T_i [K]. K_{init} [kg s^{-1} m MPa^{-1}] is initial hydraulic conductivity of each segment, ϵ_x is the maximum allowable error of the estimation of xylem water potential [MPa] and ϵ_T is the maximum allowable error of the estimation of leaf temperature [K]. Circles inside module boxes indicate internal iteration loops. Symbols between curly brackets represent spatially structured variables.

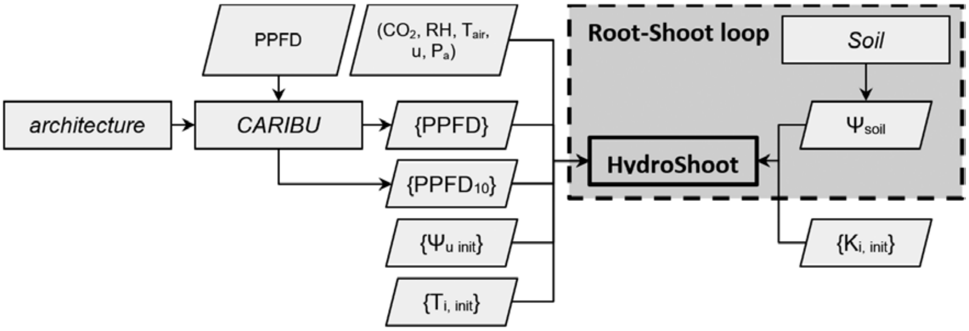

Figure 3. Flowchart of the modelling frame used in this application example. Meteorological inputs that are common to all leaves are air temperature (T_{air}, K), air relative humidity (RH, –), air CO$_2$ concentration [µmol mol^{-1}], wind speed (*u*, m s^{-1}) and atmospheric pressure (P_a, kPa). Inputs per individual leaves are the absorbed photosynthetic photon flux density (PPFD, µmol m^{-2} s^{-1}) and PPFD$_{10}$, the absorbed PPFD during the last 10 days. $\Psi_{u,init}$ is the initial xylem water potential at the nodes between each pair of hydraulic segments [MPa]. Ψ_{soil} is soil water potential. $T_{i,init}$ is initial temperature of individual leaves [K]. K_{init} [kg s^{-1} m MPa^{-1}] is initial hydraulic conductivity of each segment. Symbols between curly brackets represent spatially structured variables. *architecture*, *CARIBU* (Chelle and Andrieu 1998) and *soil* are external modules used to simulate canopy architecture, irradiance interception and soil water potential, respectively.

where i refers to leaf identifier, α_{R_g} is lumped leaf absorptance in the shortwave band [–], Φ_{R_g} is flux density of shortwave global irradiance R_g [W m^{-2}], ϵ_{leaf}, ϵ_{sky} and ϵ_{soil} are emissivity-absorptivity coefficients of the leaf, sky and soil, respectively [–], σ is the Stefan–Boltzmann constant [W m^{-2} K^{-4}], and T_{sky}, T_{soil} and T_{air} are, respectively, the sky, soil, and air absolute temperatures [K], all taken as input parameters for HydroShoot; T_j is temperature of neighbouring leaf j (solved by convergence, see Implementation and numerical resolution section), λ is latent heat for vapourization [W s mol^{-1}], K_{air} is the thermal conductivity of air [W m^{-1} K^{-1}], and finally, k_{sky}, k_{soil} and F_{ij} are the form factors of the sky, soil and canopy elements in the sphere Ω surrounding the leaf i (Chelle and Andrieu 1998). α_{R_g}, and ϵ_{leaf} are input parameters considered as uniform for all leaves.

It is noteworthy that only the forced convective heat transfer is currently considered in HydroShoot since forced convection dominates free convection once wind speed exceeds roughly 0.1 m s^{-1} (Nobel 2005). This wind speed threshold is generally exceeded during diurnal hours. However, under low wind conditions, heat transfer may be underestimated.

Since the resolution of the last equation is highly time-consuming, we assumed the energy gain from the neighbouring leaves through thermal longwave as a lumped term whereby average leaf temperature T_{leaves} is considered instead of individual leaves (Dauzat *et al.* 2001). In this case, the lumped form factor $\sum\limits_{j\in\Omega} F_{ij}$ is simply taken as $1 - (k_{sky} + k_{soil})$ (that is, the solid angle where neither the sky nor the soil are seen by a single leaf). The former equation becomes:

$$\begin{aligned}0 &= \alpha_{iR_g}\Phi_{iR_g}\\ &+ \varepsilon_{ileaf}\;\sigma\;\left(k_{isky}\;\varepsilon_{sky}\;T_{sky}^4 + k_{isoil}\;\varepsilon_{soil}\;T_{soil}^4 + \left[1-\left(k_{sky}+k_{soil}\right)\right]\;T_{leaves}^4\right)\\ &-2\;\varepsilon_{ileaf}\;\sigma\;T_i^4 - \lambda E_i - 2K_{air}\frac{(T_i - T_{air})}{\Delta x_i}\end{aligned} \tag{14}$$

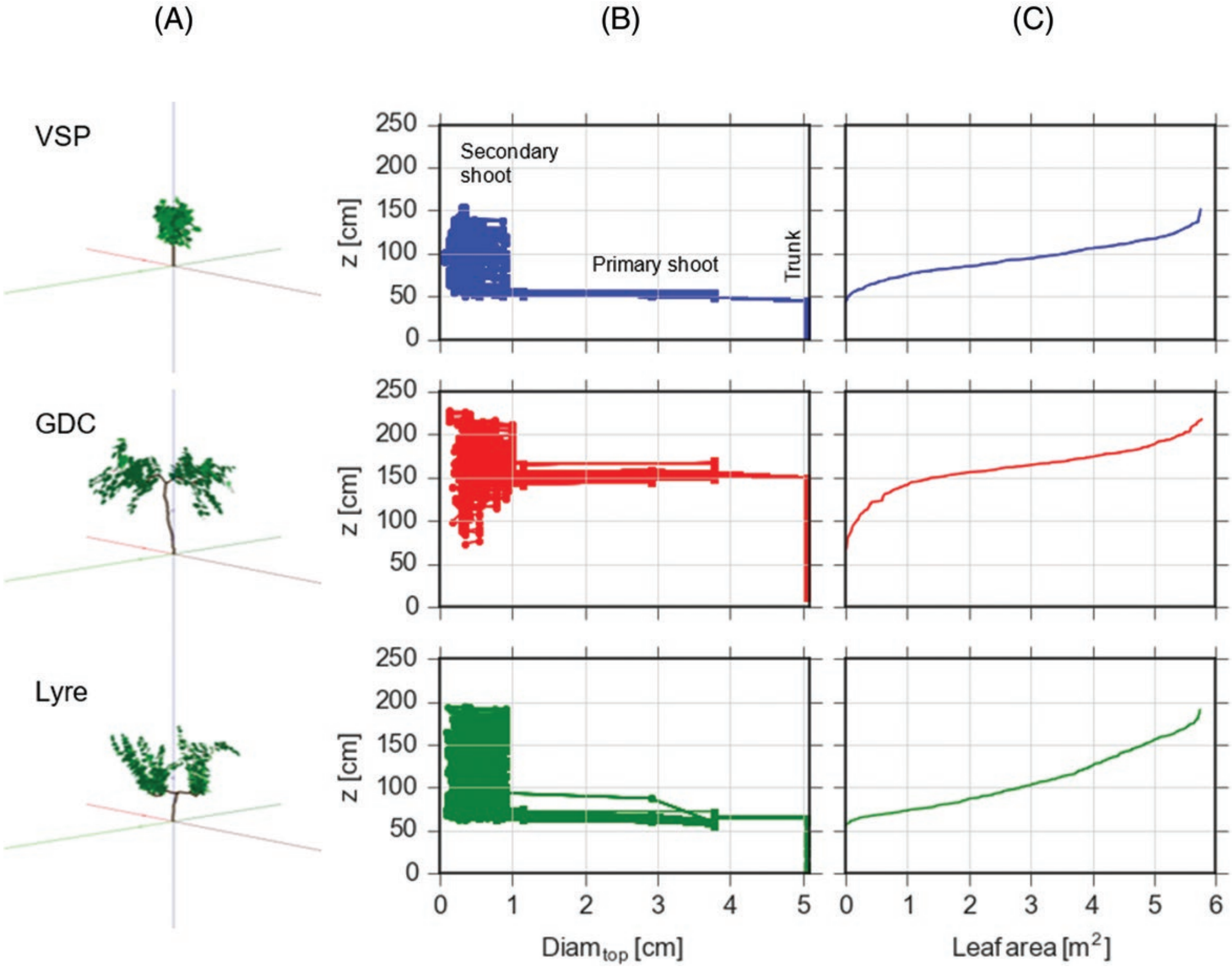

Figure 4. Mock-ups of three virtual grapevine canopies trained, respectively, to Vertical Shoot Positioning (VSP), Geneva Double Curtain (GDC) and Lyre systems. (A) Canopies mock-ups, (B) hydraulic segments (primary and secondary internodes, petioles) diameters distribution and (C) cumulative leaf area with height.

Implementation and numerical resolution

HydroShoot is developed using the *Python* programming language (Python Software Foundation: http://www.python.org) in the OpenAlea platform (Pradal *et al.* 2008, 2015). The code of the model can be freely accessed through its public depository (https://github.com/openalea/hydroshoot). It uses the Multiscale Tree Graph (MTG) method (Godin and Caraglio 1998; Balduzzi *et al.* 2017) as a central data structure in order to allow indirect communication between the different models which favours modularity (Fournier *et al.* 2010; Garin *et al.* 2014). Each process has been implemented as a reusable component in OpenAlea and can be reused independently in other models and composed in various ways, provided that the other models are written in the *Python* language and provide the adequate inputs.

The resolution of HydroShoot equations is performed by an iterative procedure that is schematized in Fig. 2.

Iterations have three levels. The first is in the *hydraulic* module and concerns calculating xylem water potential of plant segments in interaction with their hydraulic conductivity (interdependent processes, cf. equations (1) and (2)). The second level is between the *exchange* and *hydraulic* modules in order to calculate jointly gas exchanges rates and leaf water potential values (transpiration affects the hydraulic structure equation (1) while the latter affects stomatal aperture equation (5b)). The third level is between the *energy* module and both *exchange* and *hydraulic* modules, so that at each time new transpiration fluxes are calculated, leaf temperature values are updated, and the new temperature values are used to update gas exchange rates which in their turn impose new xylem water potential distribution. The details on the numerical resolution are given in Appendix 3.

Coupling with irradiance and soil models. HydroShoot needs irradiance absorption by individual leaves and soil water potential as inputs. It is therefore coupled in this work to Caribu irradiance model (Chelle and Andrieu 1998) and to a simple soil water-budget model in order to calculate, respectively, irradiance absorption (PPFD) and soil water potential (Ψ_{soil}) values on an hourly basis (Fig. 3).

The *soil* module links transpired water rates to the transpirable soil water volume (TSW) in order to predict the hourly variations in Ψ_{soil}. At the beginning of each calculation step, transpired water volume from

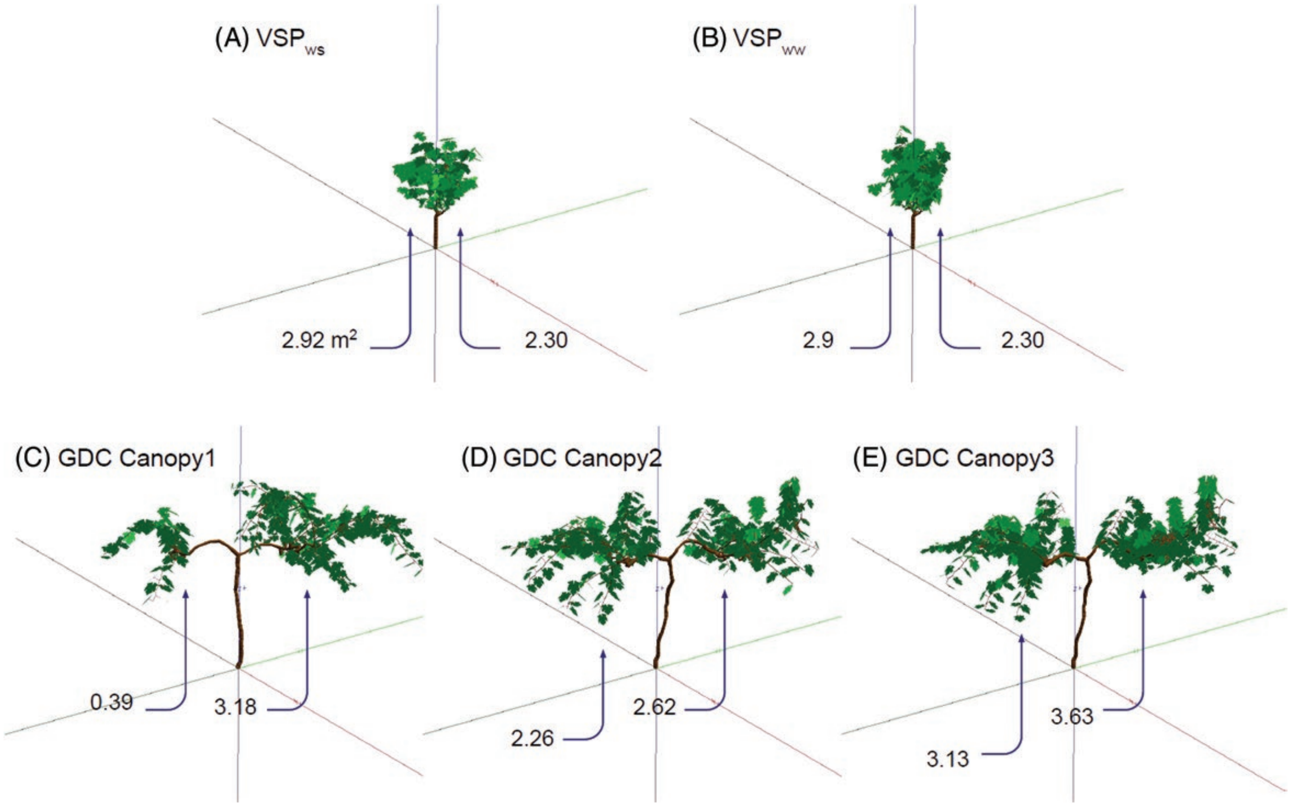

Figure 5. 3D mock-ups of grapevines plants trained to Vertical Shoot Positioning system (VSP) (A, B) under water deficit (VSP$_{WD}$), well water conditions (VSP$_{WW}$) and Geneva Double Curtain (GDC) (C–E). The mock-ups were reconstructed from measured leaf surface profiles using the *architecture* module (input to HydroShoot). Numbers below canopies indicate leaf area per cordon [m^2].

the previous step is withdrawn from the TSW. The soil volumetric water content Θ_{soil} is then determined by dividing TSW by the effective soil porosity. Ψ_{soil} is then obtained from Θ_{soil} from the water retention curve (van Genuchten 1980) and used as an input for the *hydraulic* module. This procedure is referred to as the *Root-Shoot loop* in Fig. 3.

Model evaluation

Model evaluation was performed in three steps. Firstly, the coherence between expected and simulated gas exchange, temperature and xylem water potential dynamics for different canopy architectures was assessed. Secondly, the precision was assessed by comparing model outputs to measured plant gas exchange rates and leaf stomatal conductance, water potential and temperature. Finally, the required complexity level was evaluated, whereby we sought at determining whether simulating the hydraulic structure and energy balance were (both) required in order to obtain accurate predictions of gas exchange rates at the plant scale. For all the following simulations, parameter values are given in Appendix 4.

Coherence. HydroShoot was run on three virtual grapevine canopies which share the same soil type, soil initial water content, weather conditions and total leaf area, and differ only in their shoot architecture (Fig. 4). The objective was to examine whether the model reflects the differences of shoot architecture on gas and energy exchange rates as may be expected. For instance, whether higher photosynthesis and transpiration rates are obtained for canopies absorbing higher solar irradiance flux densities. Similarly, to examine whether higher transpiration rates trigger steeper drops in leaf water potential.

The three canopies were trained on three different training systems: Vertical Shoot Positioning (VSP), Geneva Double Curtain (GDC) and Lyre systems (Fig. 4A). All canopies had the same leaf area (5.7 m^2), internode diameter distribution (Fig. 4B), planting density (inter- and intra-row spacing of 3.6 and 1.0 m, respectively), soil type (Sand Loam) and initial collar water potential (−0.6 MPa).

The simulations were run using weather data extracted from the database of the weather station of the National Institute for Agricultural Research (INRA) in

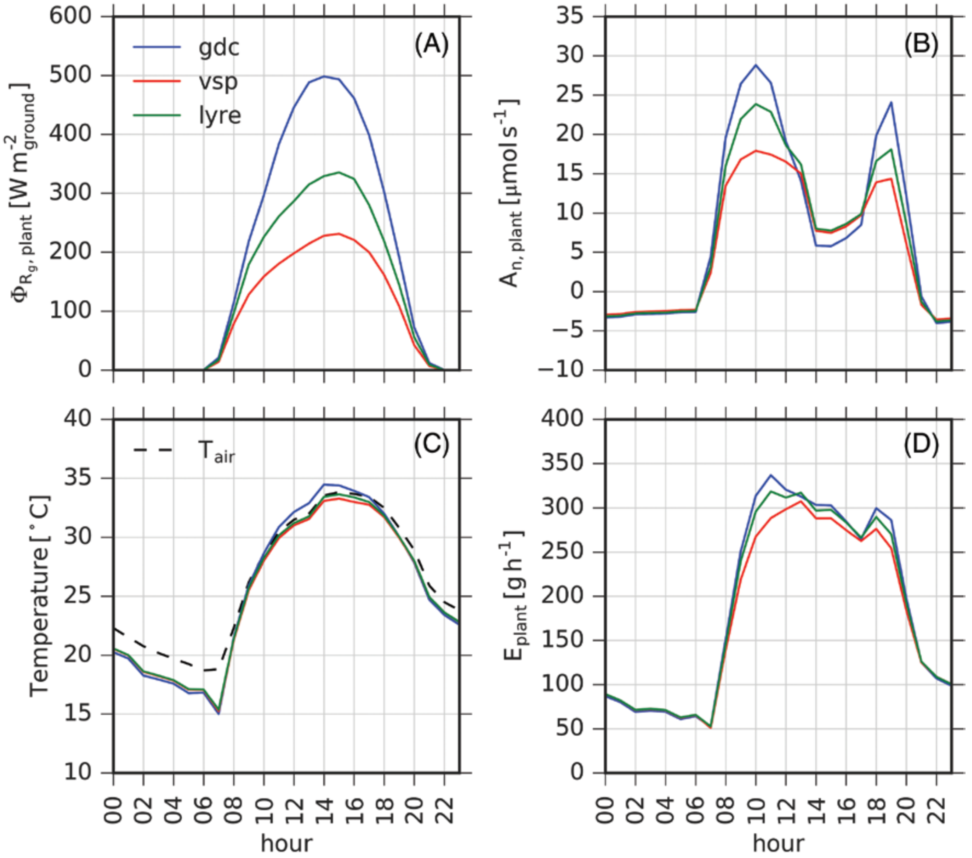

Figure 6. Simulation of absorbed irradiance (A), net carbon assimilation (B), temperature (C) and transpiration (D) at the plant scale for three contrasted grapevine canopies (VSP, GDC and Lyre); T_{air} is air temperature. Temperature curves in (C) trace the hourly values of the median of leaves temperatures.

Montpellier (3°53′′E, 43°37′′N, 44 m alt) on 29 July 2009 (DOY 210). Weather conditions corresponded to a warm day having minimum and maximum air temperature of 19 and 34 °C, respectively, relative humidity oscillating between 32 and 44 %, wind speed at 2 m height going from 0 to 2 m s^{-1}, and a clear sky with a maximum PPFD of 1670 µmol m^{-2} s^{-1} at solar midday.

Precision. The precision of simulated outputs was evaluated by running HydroShoot on real canopies using collected data from experiments conducted in 2009 and 2012 on grapevine (cv. Syrah, grafted on SO4) at INRA, in Montpellier (same above-mentioned station). Five grapevines trained with two contrasting training systems were considered (cf. Fig. 5): GDC in 2009 and VSP in 2012. Grapevine rows were oriented 140° from North on a shallow sandy loam soil with a low water holding capacity. Inter-row spacing was 3.6 m for GDC and 1.8 m for VSP. Intra-row spacing was 1 m **[see Supporting Information S4]**.

Data on VSP grapevines (2009) were collected during a period of 4 days under well-watered and water deficit conditions. Water deficit was created by cutting off the irrigation system on the first day of the experiment (July 29th). Whole plant transpiration E_{plant} and net assimilation $A_{n,plant}$ were monitored using open portable gas exchange chambers (Perez Peña and Tarara 2004). Temperature of individual leaves were monitored using thermocouples inserted into the primary veins of 10 fully developed individual leaves positioned on different heights from the top of the canopy to the inside, so that temperature gradient resulting from different irradiance conditions was captured.

Data on GDC grapevines (2012) were also collected during a 4-day experiment (starting on 1 August), but only under water deficit conditions. Only E_{plant} rate was monitored by measurements of sap flow installed on the two cordons of the GDC plants. Stomatal conductance and leaf water potential measurements were performed for a number of leaves on GDC grapevines during the experiment, but the exact position of leaves was not reported with measurements.

For both VSP and GDC grapevines, shoot architecture was constructed based on digitisation data, using a grapevine-specific shoot architecture module following

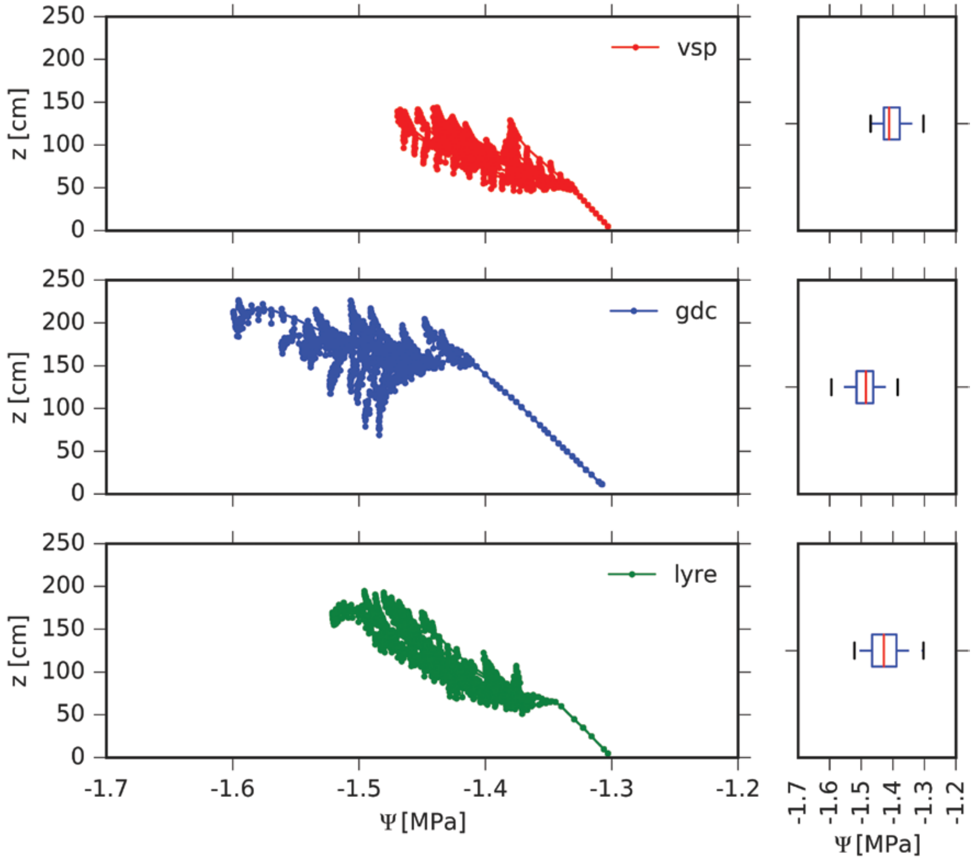

Figure 7. Snapshot at solar midday (14:00 h) of water potential distribution across the shoot (left column) and only for leaves (boxplots, right column) for three contrasted grapevine canopies (VSP, GDC and Lyre).

a Multiscale Tree Graph (MTG) approach (Godin and Caraglio 1998; Pradal *et al.* 2008; Balduzzi *et al.* 2017), in which organs topological connections and geometry were associated to shoot architecture (Fig. 5). Plant mock-ups were produced so that the simulated vertical and horizontal profiles of leaf surface area fitted those observed.

Complexity. In order to explore the contribution of HydroShoot's *hydraulic* and *energy* modules components to the final simulation output, a sensitivity analysis was performed by plugging/unplugging each of these components and observing the resulting difference on simulated outputs. This procedure aims *in fine* at evaluating whether adding complexity to an FSPM would improve its performance in predicting gas exchange dynamics at the plant scale. The following simulation combinations are used:

- sim0: the reference (complete) version of HydroShoot having the ensemble of its components;
- sim1: stomatal conductance varies with VPD (as described by Leuning 1995 in equation (5a)) regardless of leaf water potential;
- sim2: the hydraulic structure is disregarded (water potential of all leaves is forced equal to water potential at the collar) and stomatal conductance varies with collar water potential equation (5c);
- sim3: energy balance is disregarded, that is all leaves have the same temperature as that of the air;
- sim4: the same case of sim1 but using tighter control of VPD on stomatal conductance (D_0 in equation (5a) is set to 1 instead of 30 as proposed by Prieto *et al.* (2012).

Evaluation criteria. The overall adequacy between observed and simulated variables was assessed based on the estimation of the mean bias error (MBE) and root mean square error (RMSE):

$$\mathrm{MBE} = \frac{\sum_{i=1}^{n_{obs}} \left(y_{sim,i} - y_{obs,i}\right)}{n_{obs}} \tag{15}$$

$$\mathrm{RMSE} = \sqrt{\frac{\sum_{i=1}^{n_{obs}} \left(y_{sim,i} - y_{obs,i}\right)^2}{n_{obs}}} \tag{16}$$

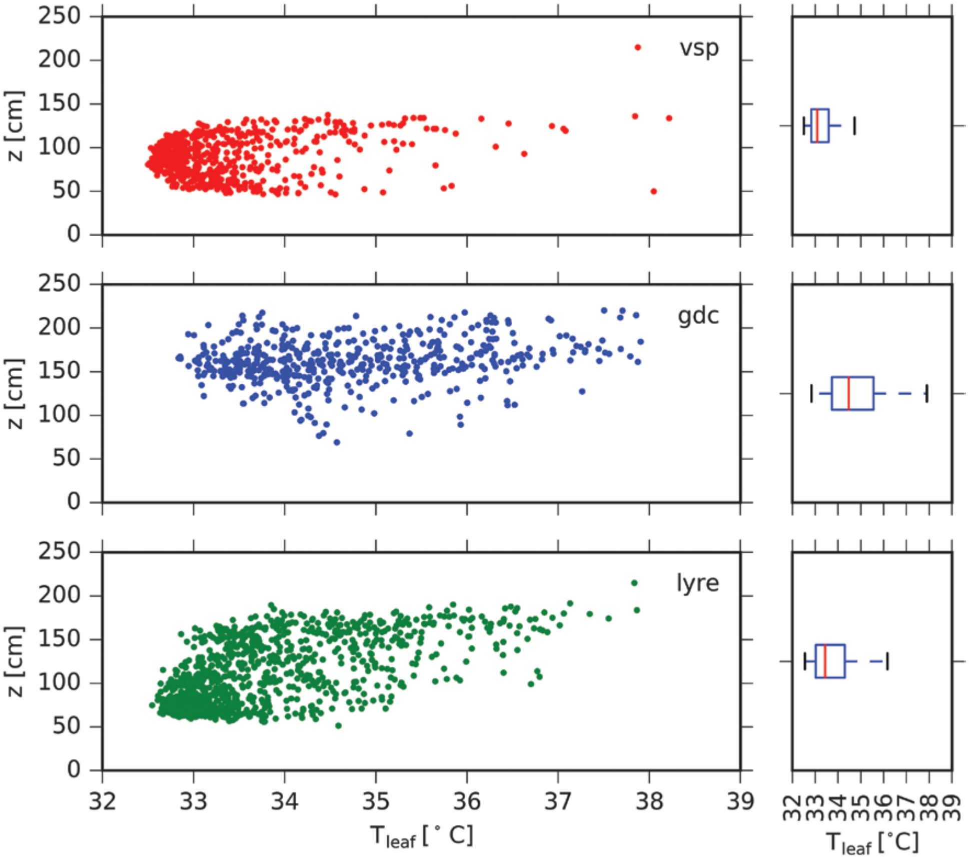

Figure 8. Snapshot at solar midday of individual leaf temperature values (left column) and leaf temperature distribution (boxplots, right column) for three contrasted grapevine canopies (VSP, GDC and Lyre).

where y_{sim} and y_{obs} are, respectively, simulated and observed variables values and n_{obs} is the number of observations.

Results and Discussion

Outputs coherence

Simulation outputs for virtual canopies are illustrated in Fig. 6 (plant-scale outputs) and Figs 7 and 8 (leaf-scale outputs).

The simulations at the plant scale (Fig. 6) show that GDC canopies had the highest absorbed irradiance rates, followed by Lyre and VSP canopies (Fig. 6A), reflecting the higher exposure to solar irradiance using the GDC system. This trend was reflected on carbon assimilation (Fig. 6B), temperature (Fig. 6C) and transpiration (Fig. 6D), whereby highest values were obtained for GDC then Lyre followed by VSP canopies.

Midday depression in $A_{n,plant}$ was simulated for the three canopies proportionally to the absorbed irradiance, that is, highest for GDC and lowest for VSP (Fig. 6B). The higher transpiration rates of GDC led to simulate lower leaf water potential values (Fig. 7) around midday, which, combined with higher absorbed irradiance, led also to higher leaf temperatures (Fig. 8). The combined effects of lower leaf water potential and higher

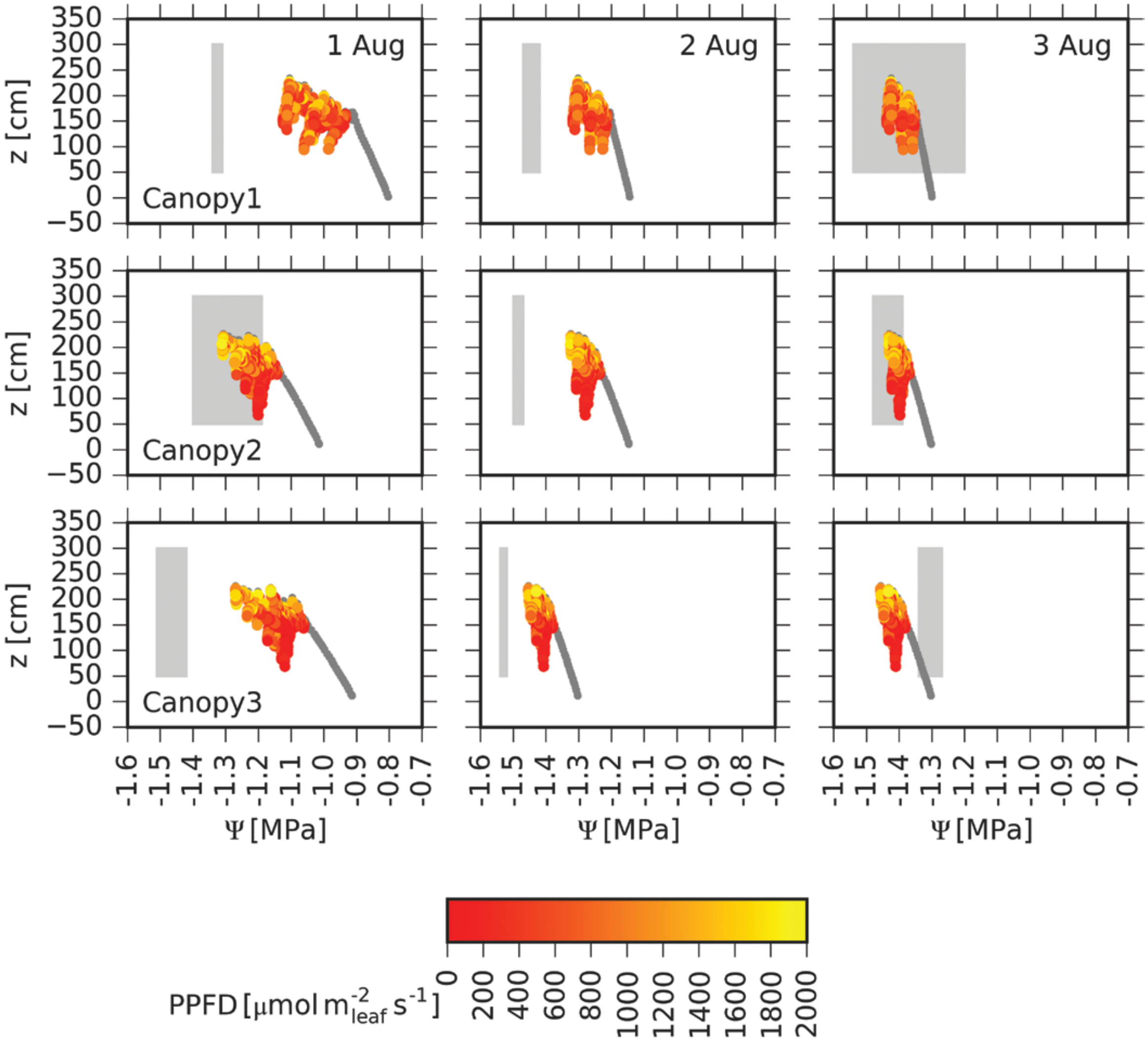

Figure 9. Snapshots of the simulated hydraulic structure of the three GDC canopies considered in this study, referred to as 'Canopy1', 'Canopy2' and 'Canopy3', respectively, prior to solar noon, during the first 3 days following the onset of soil water deficit, respectively, 1 August, 2 August and 3 August. Soil predawn water potential of the 3 days was equal to −0.19, −0.38, −0.61 MPa, respectively. Filled circles represent xylem water potential, and their colours (only for leaves) represent the absorbed PPFD value per unit leaf surface area; sunlit leaves are yellow, while shaded leaves are red, and grey circles are for the trunk. Due to uncertainties in measurements locations, the observed water potential values of sunlit leaves are indicated by the grey patches which cover minimum and maximum leaf water potential values. Observed data were collected from experiments conducted in 2012.

temperature in GDC led to simulate a higher effect of midday depression in $A_{n,plant}$ compared to Lyre and VSP canopies as may be expected.

This first illustrative example on virtual canopies shows that the effect of canopy architecture on its gas exchange and temperature behaviour is captured in HydroShoot. The comparison to measurements in the following section will show how the observed dynamics on both plant and leaf scales are accurately reproduced using HydroShoot for two real canopies.

Comparison to observed data

Leaf scale. Simulation results at the leaf scale are shown in Figs 9–11, respectively, for water potential, stomatal conductance and temperature. The dynamics of these variables were adequately reproduced but with some discrepancies regarding the onset timing of the effect of water deficit.

Figures 9 and 10 show that the simulated Ψ_{leaf} and g_{s,H_2O} of the three GDC canopies decreased progressively as the soil water deficit increased, consistently with

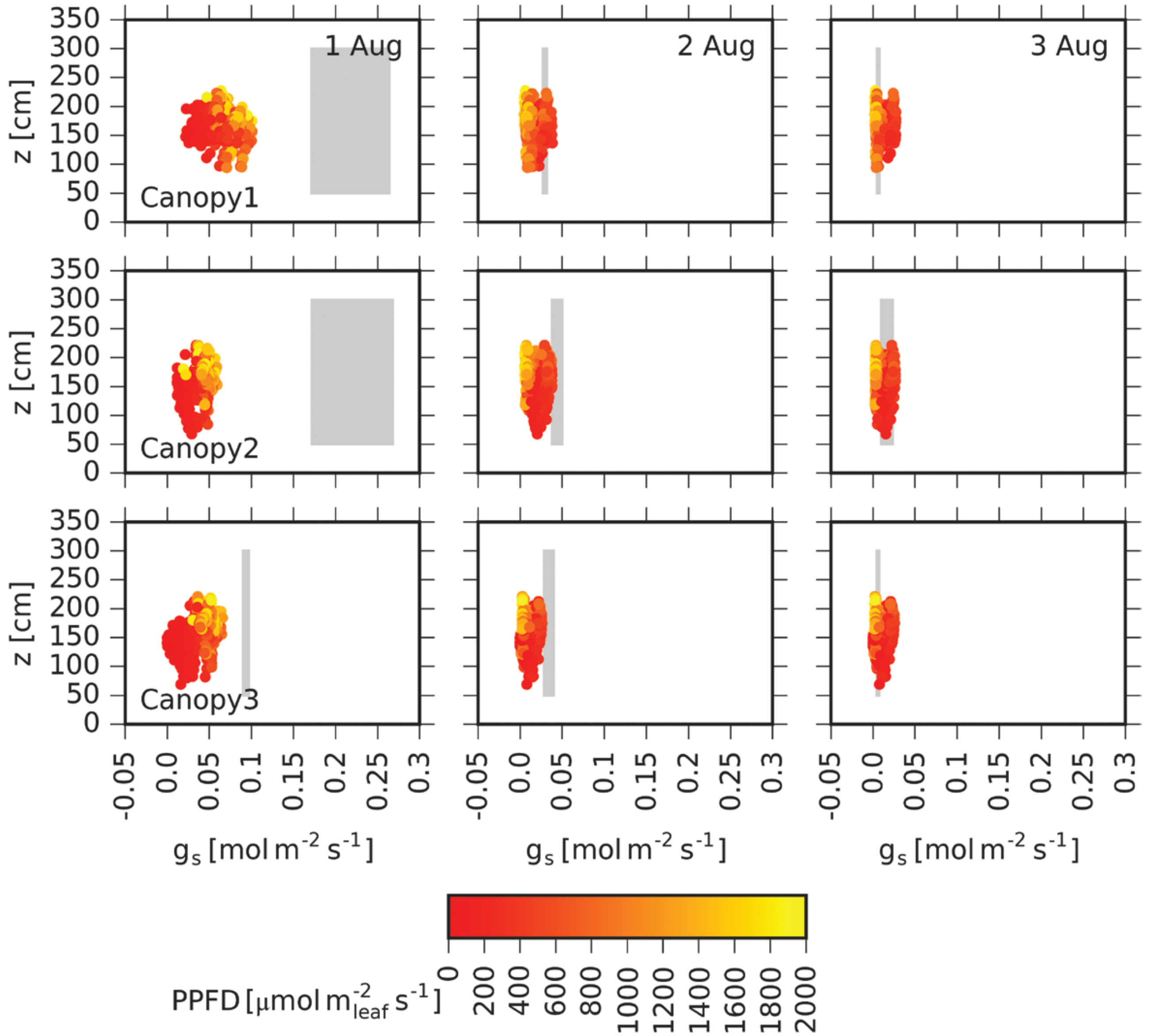

Figure 10. Snapshots of the stomatal conductance of the three GDC canopies considered in this study, referred to as 'Canopy1', 'Canopy2' and 'Canopy3', respectively, prior to solar noon, during the first 3 days following the onset of soil water deficit, respectively, 1 August, 2 August and 3 August. Soil predawn water potential of the 3 days was equal to −0.19, −0.38, −0.61 MPa, respectively. Filled circles represent stomatal conductance to water (TSW), and their colours represent absorbed PPFD value per unlit leaf surface area; sunlit leaves are yellow while shaded leaves are red. Due to uncertainties in measurements locations, the observed stomatal conductance values of sunlit leaves are indicated by the dark grey patches which cover minimum and maximum values. Observed data were collected from experiments conducted in 2012.

observations, but with an earlier onset of water stress which is probably due to inadequate parametrization either of the response function of g_{s,H_2O} to Ψ_{leaf} (cf. equation (5b)) or of the soil hydrodynamic model (cf. coupling with irradiance and soil models). Upon the onset of water stress, when water deficit was still mild in the first day (1 August in Fig. 10), HydroShoot simulated higher g_{s,H_2O} for sunlit leaves than for shaded leaves. Later, as water deficit increased, this trend was inverted, whereby sunlit leaves had the lowest g_{s,H_2O} rates (dates 2 August and 3 August in Fig. 10). This inversion was due to a lower Ψ_{leaf} for sunlit leaves as a consequence of higher potential transpiration withdrawal per unit leaf surface area (cf. equation (1)).

Moreover, Fig. 10 shows that, by the end of the water deficit period (day 3 August), leaf position had merely no more effect on its water vapour conductance g_{s,H_2O}. At this stage, water potential of all leaves reached low values at which stomata were almost closed. This uniformization of stomatal closure through the canopy is consistent with the observations reported by Escalona *et al.* (2003, 2016). Both studies reported a progressive homogenization of gas exchange rates of grapevine leaves (cv. Tempranillo, Manto Negro and Grenache) as

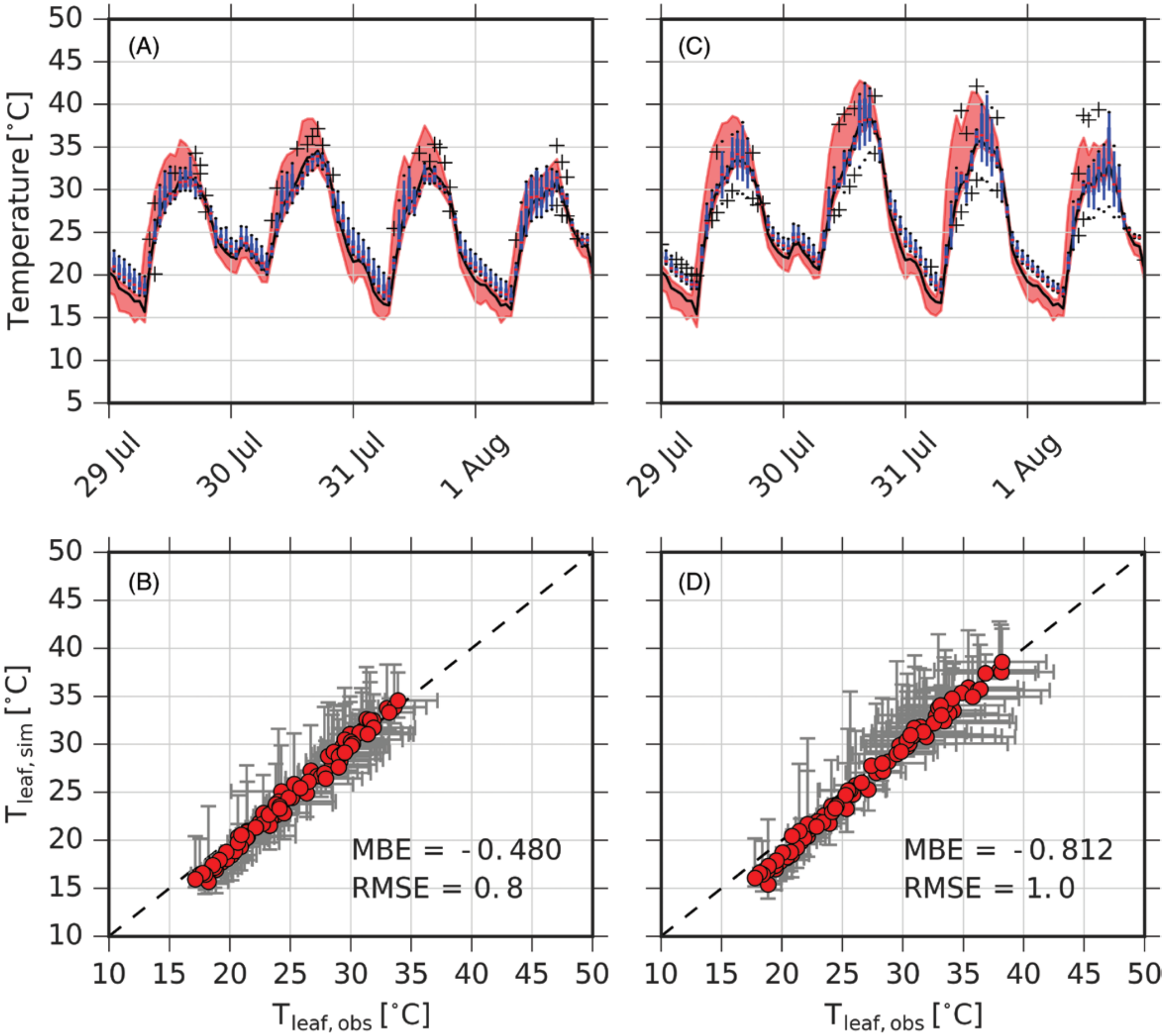

Figure 11. Comparison between simulated and observed individual leaf temperature for VSP canopies under well-watered (A, B) and water deficit (C, D) conditions. Soil predawn water potential of the 4 days was equal to −0.37, −0.50, −0.40, and −0.32 MPa respectively. (A, B) Diurnal variation in leaf temperature: red zones indicate the extension between maximum and minimum simulated values, black curves indicate simulated mean values, while blue boxplots indicate observed leaf temperature; (C, D) 1:1 plots between observed (x-axis) and simulated (y-axis) leaves median temperatures for each hour with error bars representing minimum and maximum temperature values.

soil water deficit increased. Ngao *et al.* (2017) reported similar results on apple trees (*M. pumila*), showing that intra-canopy variability in g_{s,H_2O} decreased significantly under the effect of soil water deficit.

The effect of soil water deficit on leaf temperature was efficiently captured by HydroShoot (Figs 11 and 12). The diurnal trends of leaf temperature were adequately reproduced (Fig. 11) whereby water-deficit leaves (Fig. 11B and D) had higher temperature than those well-watered (Fig. 11A and C). The comparison between simulated and observed temperatures at the leaf-level (Fig. 12) shows that the model simulated an increase in leaf-to-air temperature of approximately 2 °C, in agreement with observations (Fig. 12A). Furthermore, HydroShoot reproduced the observed magnitude between minimum and maximum leaf temperatures across the canopy (Fig. 12B) and how this magnitude increased with soil water deficit (Fig. 12C).

The overall adequation between simulated and observed leaf temperature was high when comparing median values (Fig. 11), having an MBE of −0.5 and −0.8 °C and an RMSE of 0.8 and 1.0 °C under well-watered and water deficit conditions, respectively. A greater RMSE of 2.4 °C was obtained when leaf-to-leaf comparison was performed (Fig. 12), yet, MBE remained at −0.45 °C.

It is noteworthy that leaf temperature was systematically underestimated during nocturnal hours (Figs 11 and 12). Luquet *et al.* (2003) and Bailey *et al.* (2016) reported similar trends that they explained by the frequent dysfunction of thermocouples during the night. From a modelling perspective, however, such discrepancies between simulated and observed temperatures may be explained by three possibilities. From the one hand, HydroShoot assumes flat leaves having uniform temperature across their surface, whereas strong temperature gradients occur across the surface of each individual leaf due to their three-dimensional structure (Saudreau *et al.* 2017). Thermocouples measure the temperature of only a limited fraction of leaf surface, and it is likely that the measured temperature differs from the uniform one simulated. From the other hand, HydroShoot considers only forced heat convection driven by wind speed (cf. equation (14)), which may lead to underestimate convective heat transfer during nights with low wind speed (0.02–0.2 m s^{-1} were recorded). The overall result is an underestimate leaf temperature during nocturnal hours. Finally, the error in simulated temperature may result from the assumption of a constant sky emissivity, while the latter is well known to vary with air humidity and temperature (Brunt 1932).

Plant scale. The observed daily patterns of $A_{n,plant}$ and E_{plant} were accurately reproduced under both well-watered and water deficit conditions (Fig. 13 for VSP and Fig. 14 for GDC).

For VSP canopies (Fig. 13), the reduction in soil water availability was reflected by the severe reductions in $A_{n,plant}$ and E_{plant} rates, consistently with observations but with a slight overestimation of E_{plant} (Fig. 13) under well-watered conditions. MBE and RMSE totalled, respectively, −0.1 and 5.5 µmol s^{-1} for $A_{n,plant}$ under well-watered conditions (Fig. 13A), compared to 1.0 and 3.8 µmol s^{-1}, respectively, under water deficit conditions (Fig. 13B). For E_{plant}, MBE and RMSE were, respectively, 89.5 and 141.7 g h^{-1} under well-watered conditions (Fig. 13C), compared

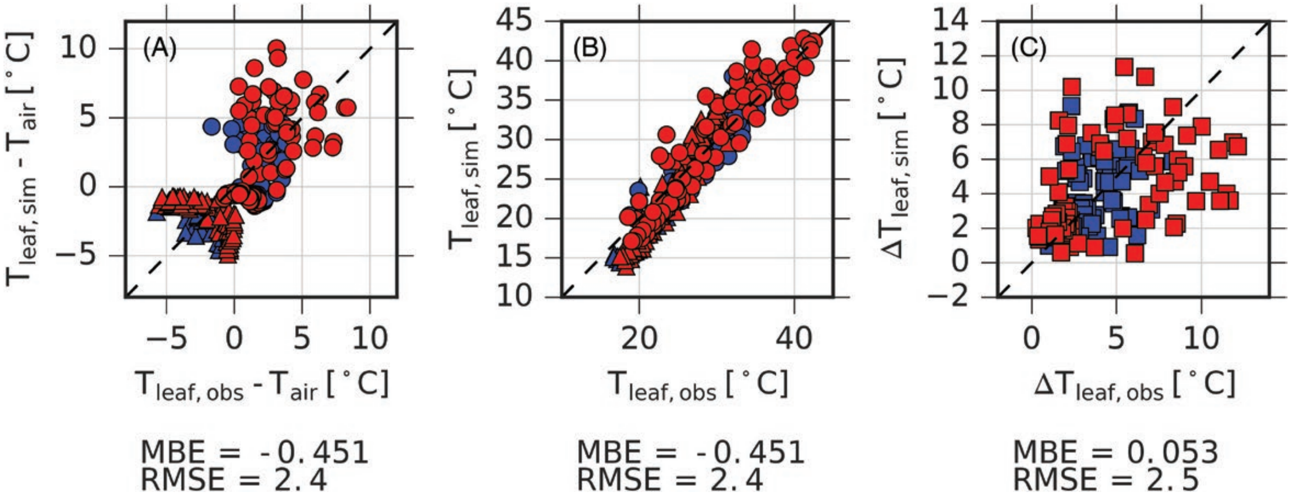

Figure 12. Comparison between the observed and simulated (A) differences between leaf and air temperatures, (B) leaf temperatures and (C) magnitude between minimum and maximum leaf temperatures across the canopy of VSP plants. Maximum and minimum leaf temperatures during each hour are represented by circles and triangles, respectively, (A and B plots), and well-watered and water deficit conditions are represented by blue and red colours, respectively.

to 27.7 and 67.6 g h^{-1}, respectively, under water deficit conditions (Fig. 13D).

For the three water-deficit GDC canopies (where only E_{plant} rates were observed), HydroShoot reasonably reproduced the diurnal patterns in E_{plant} (Fig. 14). Yet, E_{plant} rates were underestimated upon the onset of water stress (day 1 August in Fig. 14) and were slightly overestimated thereafter. MBE fall between −22.3 and 29.2 g h^{-1} and RMSE between 13.7 and 105.4 g h^{-1} which were similar to values obtained for VSP. It is noteworthy that the impact of the imbalance in leaf area between both cordons of Canopy1 (cf. Fig. 5) was reflected in the simulated E_{plant} (Fig. 14, Canopy 1) whereby a noticeable differences in the simulated fluxes was obtained between both cordons of the canopy consistently with the observed sap flow rates. This example further demonstrates how the impact of canopy is adequately reflected on its eco-physiological functioning in HydroShoot.

To which extent is modelling complexity needed?

We show in Fig. 15 together with Table 1 that the best fit between simulated and observed gas exchange rates was obtained using the complete HydroShoot model (i.e. sim0) which yielded, in almost all cases, the

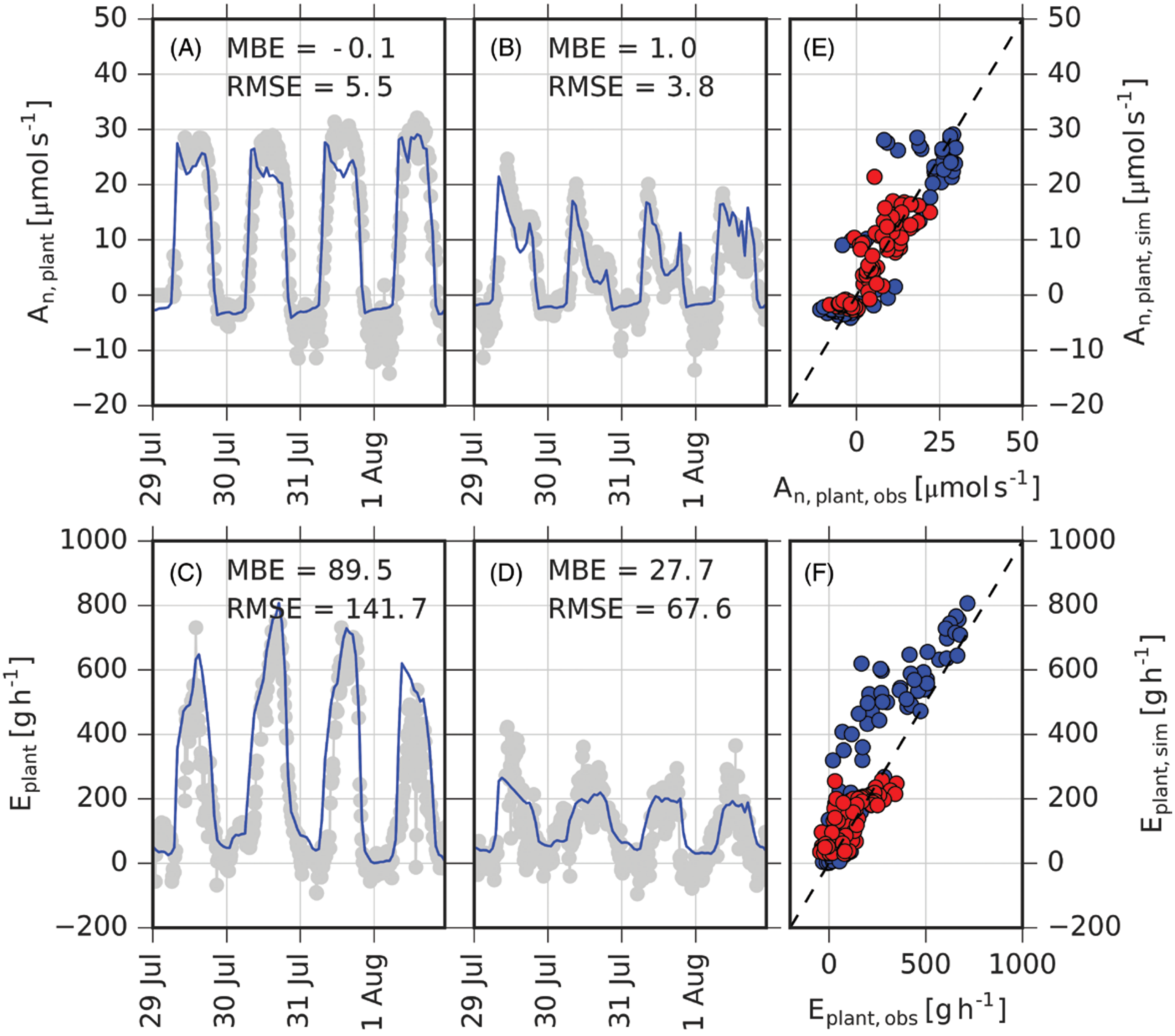

Figure 13. Comparison between simulated and observed plant net carbon assimilation ($A_{n,plant}$) and transpiration (E_{plant}) rates of VSP canopies. The subplots A–D trace the temporal trends of $A_{n,plant}$ and E_{plant} (grey circles are for observed values and blue lines are for those simulated) conducted under well-watered (A, C) and water deficit (B, D) conditions. Subplots E and F compare simulated to observed rates for both water conditions (blue dots for well-watered and red dots for water deficit). Soil predawn water potential of the 4 days was equal to −0.13, −0.15, −0.15, and −0.08, respectively, under well-watered conditions and −0.19, −0.30, −0.37, and −0.50 MPa, respectively, under water stress. MSE and RMSE indicate, respectively, mean bias error and root mean squared error (same units of the y-axes).

least values of MBE and RMSE for both $A_{n,plant}$ and E_{plant}. However, the simulated hydraulic structure and spatialized leaf temperature values had unequal contributions to prediction's accuracy.

When stomatal aperture was dissociated from soil water status (i.e. sim1 and sim4), the results indicated a substantial increase in prediction errors, resulting in particular in the highest values for both MBE and RMSE for E_{plant}. For instance, RMSE increased from 142 to 361 g h^{-1} under well-watered conditions, and from 68 to 315 g h^{-1} under water deficit conditions, when sim0 is compared to sim1. An improvement in prediction quality was obtained when stomatal aperture was linked to the collar water potential Ψ_{collar} (i.e. sim2), yet, a considerable error still existed compared to the reference case. For instance, MBE of $A_{n,plant}$ increased from −0.05 to 1.26 µmol s^{-1} and from 1.01 to 3.53 µmol s^{-1}, respectively, under well-watered and water deficit conditions, with sim2 compared to sim0. Similarly, MBE of E_{plant} increased from 89 to 170 g h^{-1} and from 28 to 35 g h^{-1}, respectively, under well-watered and water deficit conditions, using sim2 compared to the reference case sim0.

This result confirms the central role played by the hydraulic structure on tightening stomatal conductance in a species well known for its conservative behaviour towards water deficit (i.e. iso- or near-isohydric, Jacobsen *et al.* 2015). It indicates that linking leaf-scale stomatal aperture to leaf-level water potential (through Ψ_{leaf}), by simulating the hydraulic structure,

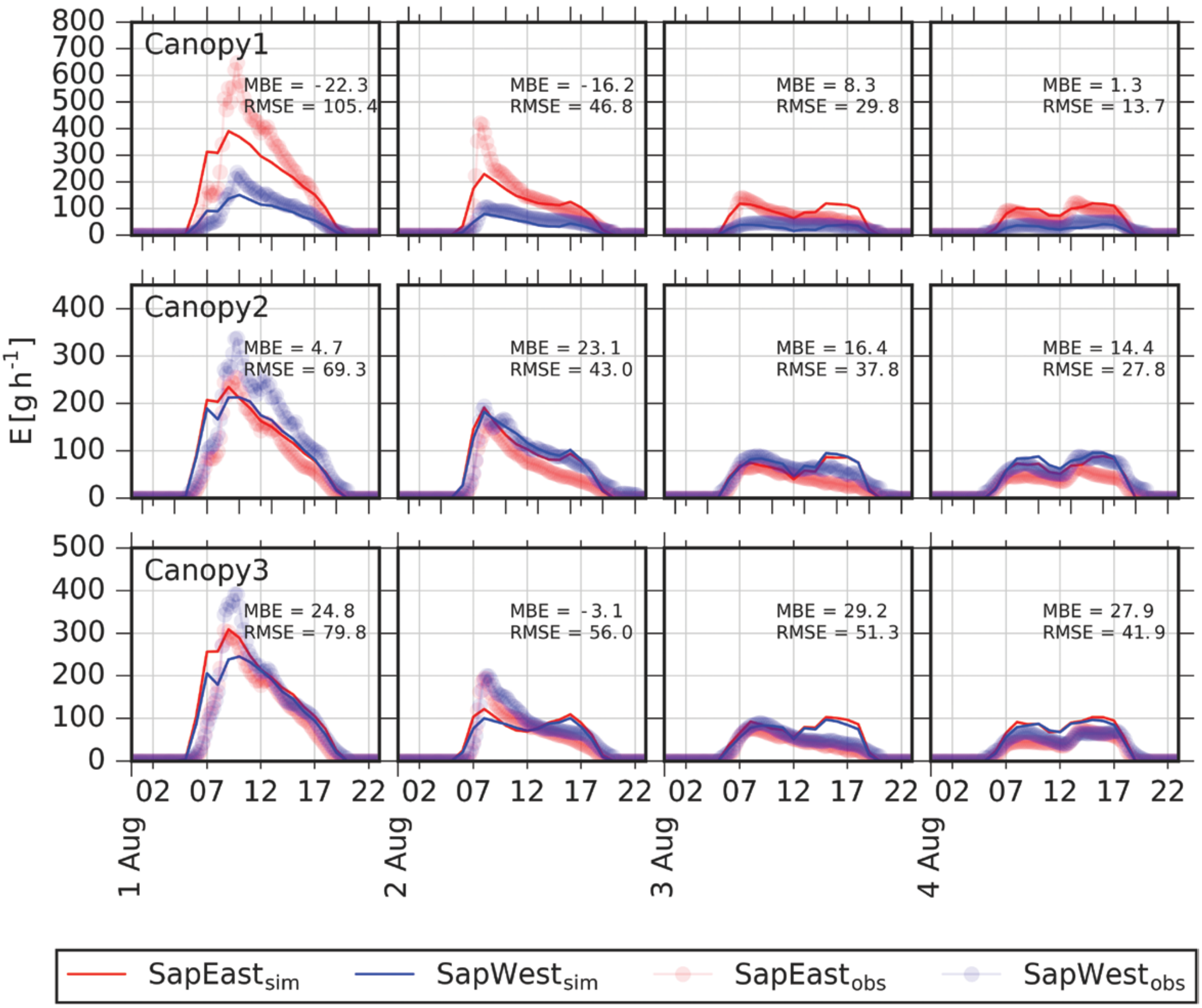

Figure 14. Comparison between the observed (circles) and simulated (curves) transpiration rates (E_{plant}) for each cordon of three grapevines plants trained to GDC under water deficit conditions. Soil predawn water potential of the three canopies was equal to −0.19, −0.38, −0.61, and −0.51 MPa, respectively. Red and blue colours indicate fluxes through east- and west-exposed cordons, respectively. MSE and RMSE indicate, respectively, mean bias error and root mean squared error (same units of the y-axes).

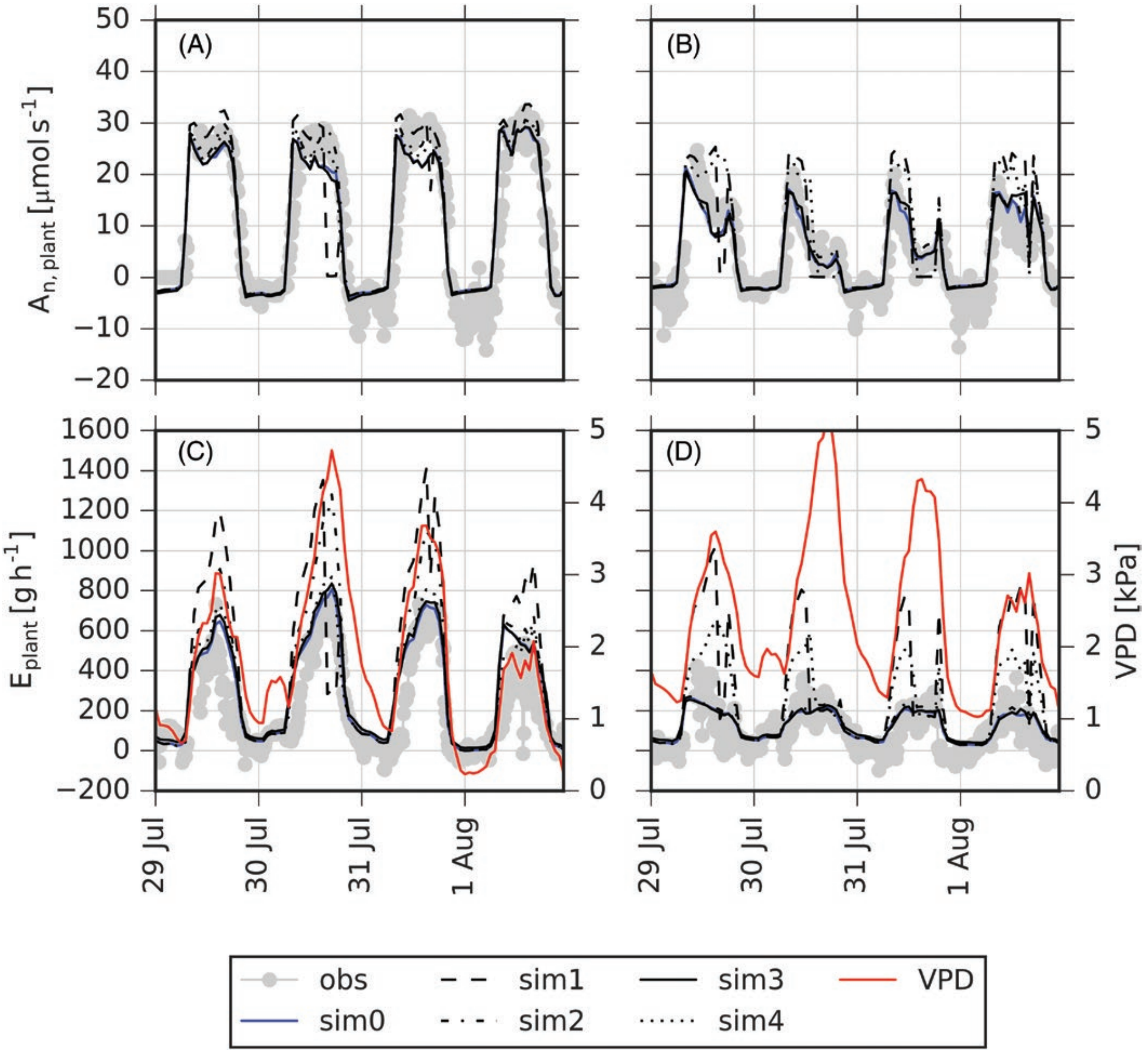

Figure 15. Impact of different modelling details of HydroShoot on the simulated plant carbon assimilation ($A_{n,plant}$) and transpiration (E_{plant}) rates: the reference (complete) HydroShoot version is indicated as sim0, sim1 indicates the version whereby leaf stomatal conductance varies with vapour pressure deficit instead of leaf water potential (i.e. original model of Leuning 1995, D_0 = 5 in equation (5a)), sim2 indicates the results obtained when the shoot hydraulic structure was omitted (i.e. all leaves have the same water potential which is equal to that of the collar), sim3 is for results obtained by omitting energy balance of individual leaves (i.e. leaves temperature equal to air temperature) and sim4 is the same as sim1 but with an increased impact of the vapour pressure deficit on VPD (D_0 = 1 in equation (5a)), and finally, obsMBEand VPD indicate, respectively, the observed gas rate and air vapour pressure deficit.

brings a considerable improvement to model performance. That is, predicting the intra-canopy variability in leaf water potential improves prediction accuracy of gas exchange rates at the whole plant scale. This result agrees with the conclusions reported by Ngao *et al.* (2017) on the role of leaf water potential variability on apple tree gas exchange rates. The authors firstly reported that a reliable prediction of plant-scale gas exchange fluxes in apple trees was allowed when stomatal closure was simulated as a function of soil water potential. However, they postulated that further improvements are yet expected when the hydraulic structure of the shoot is simulated.

Regarding the contribution of simulating leaf-scale energy balance to the predicted plant-scale fluxes, its effect was shown weak (Table 1). Indeed, disregarding energy balance calculations (i.e. sim3) merely affected the predicted $A_{n,plant}$ rates under both water conditions. For the well-watered case, MBE and RMSE changed from of −0.05 to −0.26 µmol s^{-1} and from 5.5 to 5.6 µmol s^{-1}, respectively, using sim0 compared to sim3. For the water deficit case, MBE changed from of 1.01 to 1.05 µmol s^{-1} while RMSE merely changed. Similar results were also obtained for E_{plant}.

Our results disagree with those reported by Bauerle *et al.* (2007) who estimated that disregarding the

Table 1. Precision estimators of simulated carbon assimilation ($A_{n,plant}$) and transpiration (E_{plant}) rates of the plant of well-watered and water-deficit VSP grapevines using five versions of HydroShoot: sim0, the reference (complete) HydroShoot version, sim1, the version whereby leaf stomatal conductance varies with vapour pressure deficit instead of leaf water potential (i.e. original model of Leuning 1995, $D_0 = 5$ in equation (5a)), sim2, shoot hydraulic structure omitted (i.e. all leaves have the same water potential which is equal to that of the collar), sim3, energy balance of individual leaves omitted (i.e. leaves temperature equal to air temperature) and sim4, the same as sim1 but with an increased impact of the vapour pressure deficit on y_{sim} ($D_0 = 1$ in equation (5a)).

		$A_{n,plant}$		E_{plant}	
		MBE	**RMSE**	**MBE**	**RMSE**
		[µmol s^{-1}]	**[µmol s^{-1}]**	**[g h^{-1}]**	**[g h^{-1}]**
WW	sim0	−0.05	5.49	89.47	141.66
	sim1	1.26	7.43	225.00	361.18
	sim2	1.20	5.27	170.15	247.45
	sim3	−0.26	5.58	109.18	154.60
	sim4	0.50	5.40	100.04	156.68
WD	sim0	1.01	3.76	27.65	67.57
	sim1	3.03	6.95	193.89	315.41
	sim2	1.36	3.86	35.41	71.13
	sim3	1.05	3.82	34.12	70.81
	sim4	3.16	6.07	127.40	196.02

Table 2. Estimation of computation cost for two canopies and three HydroShoot versions (sim0, the complete HydroShoot version, sim3, energy balance of individual leaves omitted (i.e. leaves temperature equal to air temperature) and sim4, leaf stomatal conductance varies with vapour pressure deficit instead of leaf water potential).

Training system	**Water condition**	**Leaf area [m^2 plant^{-1}]**	**Computation time (per time step) [s]**		
			sim0	sim3	sim4
VSP$_{ww}$	well-watered	5.2	11.96	2.98	19.87
GDC (Canopy 1)	water deficit	3.56	7.45	2.29	26.57

intra-canopy variability in leaf temperature would lead to overestimate E_{plant} by 22–25 % for red maple (*A. rubrum*). In our case study on grapevine, disregarding leaf energy balance calculations increased the simulated E_{plant} by no more than 9% **[see Supporting Information S5]**. The differences between our results and those reported by Bauerle *et al.* (2007) may rely on the way the authors accounted for the impact of microclimate inside the canopy on leaf photosynthetic traits. In their study, Bauerle *et al.* (2007) used leaf temperature as the primer driver for intra-canopy variability in leaf photosynthetic traits. In our study, we linked leaf photosynthetic traits to the 10-day cumulative absorbed PPFD (cf. equation (12)) while leaf temperature was used only to affect directly A_n, and indirectly g_{s,H_2O}. This conceptual difference may explain the lower sensitivity to leaf temperature in our study compared to that performed by Bauerle *et al.* (2007). Bailey *et al.* (2016) showed furthermore that the importance of accounting for the intra-canopy distribution of leaf temperature in FSPMs is a matter of canopy size. The authors reported that for grapevines, leaf temperature distribution had a negligible impact on the simulated plant-scale emitted thermal longwave irradiance. In contrast, on Freeman maple (*Acer* × *freemanii*) which have notably higher leaf area per plant, simulating the spatial distribution of leaf temperature reduced by 50% prediction errors of the emitted thermal longwave irradiance. The low sensitivity of HydroShoot to leaf temperature may thus be linked to the simulated canopy size.

Notwithstanding, it is noteworthy that omitting energy balance calculations in HydroShoot allowed saving up to 75% compared to the case where all processes combination was considered (Table 2). Using the complete combination (sim0) is indeed quite costly in time (between 7 and 12 s for each simulation time step, i.e. hour). Removing the energy balance reduced considerably time cost (by up to 75% in the case of VSP) and reduced non-convergence risk (data not show). Removing the hydraulic structure (i.e. stomata are only function of VDP, sim4) increased considerably the time required for convergence (60% for VSP and up to 250% for the water-deficit GDC Canopy 1) and non-convergence risk. The considerable economy in calculation cost is an argument that should be considered when simulating large-scale plant scenes.

Data

All data used in this paper are available from HydroShoot open-access depository through the OpenAlea platform (https://github.com/openalea/hydroshoot).

Conclusions

We presented in this paper the FSPM HydroShoot. This model was built in order to allow simulating the effect of plant shoot architecture on its gas exchange dynamics under soil water deficit conditions. In order to achieve this objective, we constructed HydroShoot on the base of three interacting processes: leaf-scale gas exchange, leaf-scale energy balance and internode-scale xylem transport (i.e. the hydraulic structure of the shoot). The produced model was evaluated using both virtual and real grapevine canopies of three strongly contrasting shoot architectures, under both well-watered and water deficit conditions. We showed that HydroShoot reproduced efficiently the effect of canopy architecture on plant-scale gas exchange processes under the observed gradient of water deficit conditions, fulfilling thus the objectives for which the model was built. We showed furthermore that both hydraulic structure and energy balance simulations were required for a precise prediction of plant-scale gas exchange rates under soil water deficit. However, our results indicate that under the given grapevine architecture, soil type and meteorological conditions, the hydraulic structure has, by far, the largest effect on simulated net photosynthesis and transpiration rates while simulating leaf-scale energy balance improves minorly prediction results.

Sources of Funding

This research was funded by the European Community's Seventh Framework Program (FP7/2007–2013) under the grant agreement no. FP7-311775, Project INNOVINE. It was also partly funded by the Environment and Agronomy Department of the French National Institute for Agricultural Research (INRA).

Conflict of Interest

None declared.

Acknowledgements

The authors greatly acknowledge Mr Gerardo Lopez for his concise and constructive notes on this manuscript. They also thank Dr Junqi Zhu for his valuable feedback on the gas exchange code. The authors dedicate this work to their beloved colleague Eric Lebon, who left us just before the closure of the INNOVINE project.

Supporting Information

The following additional information is available in the online version of this article—

Supporting Information S1. Comparison to existing FSPMs.

Supporting Information S2. Effects of temperature and irradiance on gas exchange rates.

Supporting Information S3. Development of the energy module.

Supporting Information S4. Description of data collection for model calibration and evaluation.

Supporting Information S5. Quantification of energy balance contribution.

Literature Cited

Bailey B, Stoll R, Pardyjak E, Miller N. 2016. A new three-dimensional energy balance model for complex plant canopy geometries: model development and improved validation strategies. *Agricultural and Forest Meteorology* **218–219**:146–160.

Balduzzi M, Binder BM, Bucksch A, Chang C, Hong L, Iyer-Pascuzzi AS, Pradal C, Sparks EE. 2017. Reshaping plant biology: qualitative and quantitative descriptors for plant morphology. *Frontiers in Plant Science* **8**:117.

Ball J, Woodrow I, Berry J. 1987. A model predicting stomatal conductance and its contribution to the control of photosynthesis under different environmental conditions. In: Biggins J, ed. Progress in Photosynthesis Research: Volume 4 Proceedings of the VIIth International Congress on Photosynthesis Providence, Rhode Island, 221–224.

Bauerle WL, Bowden JD, Wang GG. 2007. The influence of temperature on within-canopy acclimation and variation in leaf photosynthesis: spatial acclimation to microclimate gradients among climatically divergent *Acer rubrum* L. genotypes. *Journal of Experimental Botany* **58**:3285–3298.

Brunt D. 1932. Notes on radiation in the atmosphere. *Quarterly Journal of the Royal Meteorological Society* **58**:389–418.

Buckley T, Mott K, Farquhar G. 2003. A hydromechanical and biochemical model of stomatal conductance. *Plant, Cell and Environment* **26**:1767–1785.

Chelle M. 2005. Phylloclimate or the climate perceived by individual plant organs: what is it? How to model it? What for? *New Phytologist* **166**:781–790.

Chelle M, Andrieu B. 1998. The nested radiosity model for the distribution of light within plant canopies. *Ecological Modelling* **111**:75–91.

Correia M, Chaves M, Pereira J. 1990. Afternoon depression in photosynthesis in grapevine leaves—evidence for a high light stress effect. *Journal of Experimental Botany* **41**:417–426.

Damour G, Vandame M, Urban L. 2010. Long-term drought results in a reversible decline in photosynthetic capacity in mango leaves, not just a decrease in stomatal conductance. *Tree Physiology* **29**:675–684.

Dauzat J, Rapidel B, Berger A. 2001. Simulation of leaf transpiration and sap flow in virtual plants: model description and application to a coffee plantation in Costa Rica. *Agricultural and Forest Meteorology* **109**:143–160.

Duchêne E, Huard F, Pieri P. 2014. Grapevine and climate change: what adaptations of plant material and training systems should we anticipate? *Journal International des Sciences de la Vigne et du Vin* 61–69.

Escalona J, Flexas J, Bota J, Medrano H. 2003. Distribution of leaf photosynthesis and transpiration within grapevine canopies under different drought conditions. *Vitis* **42**:57–64.

Escalona J, Pou A, Tortosa I, Hernández-Montes E, Tomás M, Martorell S, Bota J, Medrano H. 2016. Using whole-plant chambers to estimate carbon and water fluxes in field-grown grapevines. *Theoretical and Experimental Plant Physiology* **28**:241–254.

Evers JB, Vos J, Yin X, Romero P, van der Putten PE, Struik PC. 2010. Simulation of wheat growth and development based on organ-level photosynthesis and assimilate allocation. *Journal of Experimental Botany* **61**:2203–2216.

Farquhar GD, von Caemmerer S, Berry JA. 1980. A biochemical model of photosynthetic CO_2 assimilation in leaves of C3 species. *Planta* **149**:78–90.

Flexas J, Medrano H. 2002. Drought-inhibition of photosynthesis in C3 plants: stomatal and non-stomatal limitations revisited. *Annals of Botany* **89**:183–189.

Fournier C, Pradal C, Louarn G, Combes D, Soulié J, Luquet D, Boudon F, Chelle M. 2010. Building modular FSPM under OpenAlea: concepts and applications. In: DeJong T, DaSilva D, eds. *Proceedings of the 6th International Workshop on Functional-Structural Plant Models*. Davis: University of California, 109–112.

Garin G, Fournier C, Andrieu B, Houlès V, Robert C, Pradal C. 2014. A modelling framework to simulate foliar fungal epidemics using functional-structural plant models. *Annals of Botany* **114**:795–812.

Godin C, Caraglio Y. 1998. A multiscale model of plant topological structures. *Journal of Theoretical Biology* **191**:1–46.

Gonzalez-Dugo V, Zarco-Tejada P, Berni J, Suarez L, Goldhamer D, Fereres E. 2012. Almond tree canopy temperature reveals intra-crown variability that is water stress-dependent. *Agricultural and Forest Meteorology* **154**:156–165.

Gutschick V. 2016. Leaf energy balance: basics, and modeling from leaves to canopies. In: Hikosaka K, Niinemets U, Anten N, eds. *Canopy photosynthesis: from basics to applications*. Dordrecht: Springer Netherlands, 23–58.

Hannah L, Roehrdanz P, Ikegami M, Shepard A, Shaw M, Tabor G, Zhi L, Marquet P, Hijmans R. 2013. Climate change, wine, and conservation. *Proceedings of the National Academy of Sciences of the USA* **110**:6907–6912.

Jacobsen AL, Pratt RB. 2012. No evidence for an open vessel effect in centrifuge-based vulnerability curves of a long-vesselled liana (*Vitis vinifera*). *New Phytologist* **194**:982–990.

Jacobsen A, Rodriguez-Zaccaro F, Lee T, Valdovinos J, Toschi H, Martinez J, Pratt R. 2015. Grapevine xylem development, architecture, and function. In: Hacke U, ed. *Functional and ecological xylem anatomy*. Cham: Springer International Publishing, 133–162.

Leuning R. 1995. A critical appraisal of a combined stomatal-photosynthesis model for C3 plants. *Plant, Cell and Environment* **18**:339–355.

Leuning R, Tuzet A, Perrier A. 2004. Stomata as part of the soil-plant-atmosphere continuum. In: Mencuccini M, Grace J, Moncrieff J, McNaughton K, eds. *Forests at the land-atmosphere interface*. Edinburgh: CABI Publishing, 9–28.

Louarn G, Lecoeur J, Lebon E. 2008. A three-dimensional statistical reconstruction model of grapevine (*Vitis vinifera*) simulating canopy structure variability within and between cultivar/training system pairs. *Annals of Botany* **101**:1167–1184.

Lovisolo C, Perrone I, Carra A, Ferrandino A, Flexas J, Medrano H, Schubert A. 2010. Drought-induced changes in development and function of grapevine (*Vitis* spp.) organs and in their hydraulic and non-hydraulic interactions at the whole-plant level: a physiological and molecular update. *Functional Plant Biology* **37**:98–116.

Luquet D, Bégué A, Vidal A, Dauzat J, Clouvel P. 2003. 3D simulation of directional temperature variability within a row-cotton crop: toward an improvement of experimental crop water status monitoring using thermal infrared. *Precision Agriculture* **4**:297–309.

Maes WH, Steppe K. 2012. Estimating evapotranspiration and drought stress with ground-based thermal remote sensing in agriculture: a review. *Journal of Experimental Botany* **63**:4671–4712.

Medrano H, Pou A, Tomás M, Martorell S, Gulias J, Flexas J, Escalona J. 2012. Average daily light interception determines leaf water use efficiency among different canopy locations in grapevine. *Agricultural Water Management* **114**:4–10.

Medrano H, Tomás M, Martorell S, Escalona J, Pou A, Fuentes S, Flexas J, Bota J. 2015a. Improving water use efficiency of vineyards in semi-arid regions: a review. *Agronomy for Sustainable Development* **35**:499–517.

Medrano H, Tomás M, Martorell S, Flexas J, Hernández E, Rosselló J, Pou A, Escalona J, Bota J. 2015b. From leaf to whole-plant water use efficiency (WUE) in complex canopies: limitations of leaf WUE as a selection target. *The Crop Journal* **3**:220–228.

Misson L, Panek JA, Goldstein AH. 2004. A comparison of three approaches to modeling leaf gas exchange in annually drought-stressed ponderosa pine forests. *Tree Physiology* **24**:529–541.

Ngao J, Adam B, Saudreau M. 2017. Intra-crown spatial variability of leaf temperature and stomatal conductance enhanced by drought in apple tree as assessed by the RATP model. *Agricultural and Forest Meteorology* **237–238**:340–354.

Niinemets Ü, Keenan TF, Hallik L. 2015. A worldwide analysis of within-canopy variations in leaf structural, chemical and physiological traits across plant functional types. *New Phytologist* **205**:973–993.

Nikolov N, Massman W, Schoettle A. 1995. Coupling biochemical and biophysical processes at the leaf level: an equilibrium photosynthesis model for leaves of C3 plants. *Ecological Modelling* **80**:205–235.

Nobel P. 2005. Temperature and energy budgets. In: Nobel S, ed. *Physicochemical and environmental plant physiology*, 4th edn. San Diego, CA: Elsevier Academic Press, 307–350.

Palliotti A, Tombesi S, Silvestroni O, Lanari V, Gatti M, Poni S. 2014. Changes in vineyard establishment and canopy management urged by earlier climate-related grape ripening: a review. *Scientia Horticulturae* **178**:43–54.

Perez Peña J, Tarara J. 2004. A portable whole canopy gas exchange system for several mature field-grown grapevines. *Vitis* **43**:7–14.

Pradal C, Dufour-Kowalski S, Boudon F, Fournier C, Godin C. 2008. OpenAlea: a visual programming and component-based software platform for plant modelling. *Functional Plant Biology* **35**:751–760.

Pradal C, Fournier C, Valduriez P, Cohen-Boulakia S. 2015. OpenAlea: scientific workflows combining data analysis and simulation. In: *Proceedings of the International Conference on Scientific and Statistical Database Management*, San Diego, 1–6.

Prieto JA, Louarn G, Perez Peña J, Ojeda H, Simonneau T, Lebon E. 2012. A leaf gas exchange model that accounts for intra-canopy variability by considering leaf nitrogen content and local acclimation to radiation in grapevine (*Vitis vinifera* L.). *Plant, Cell & Environment* **35**:1313–1328.

Reynolds A, Vanden Heuvel J. 2009. Influence of grapevine training systems on vine growth and fruit composition: a review. *American Journal of Enology and Viticulture* **60**:251–268.

Saudreau M, Ezanic A, Adam B, Caillon R, Walser P, Pincebourde S. 2017. Temperature heterogeneity over leaf surfaces: the contribution of the lamina microtopography. *Plant Cell and Environment* **40**: 2174–2188.

Tuzet A, Perrier A, Leuning R. 2003. A coupled model of stomatal conductance, photosynthesis and transpiration. *Plant, Cell and Environment* **26**:1097–1116.

Tyree M, Sperry J. 1989. Vulnerability of xylem to cavitation and embolism. *Annual Review of Plant Physiology and Plant Molecular Biology* **40**:19–38.

Tyree M, Zimmermann M. 2002. *Xylem structure and the ascent of sap, Springer series in wood science*, Heidelberg.

van Genuchten M. 1980. A closed-form equation for predicting the hydraulic conductivity of unsaturated soils. *Soil Science Society of America Journal* **44**:892–898.

van Leeuwen C, Philippe D. 2016. The impact of climate change on viticulture and wine quality. *Journal of Wine Economics* **11**:150–167.

van Wijk MT, Dekker SC, Bouten W, Bosveld FC, Kohsiek W, Kramer K, Mohren GM. 2000. Modeling daily gas exchange of a Douglas-fir forest: comparison of three stomatal conductance models with and without a soil water stress function. *Tree Physiology* **20**:115–122.

Vos J, Evers JB, Buck-Sorlin GH, Andrieu B, Chelle M, de Visser PH. 2010. Functional-structural plant modelling: a new versatile tool in crop science. *Journal of Experimental Botany* **61**:2101–2115.

Yin X, Struik P. 2009. C3 and C4 photosynthesis models: an overview from the perspective of crop modelling. *NJAS - Wageningen Journal of Life Sciences* **57**:27–38.

Zhu J, Dai Z, Vivin P, Gambetta GA, Henke M, Peccoux A, Ollat N, Delrot S. 2018. A 3-D functional-structural grapevine model that couples the dynamics of water transport with leaf gas exchange. *Annals of Botany* **121**:833–848.

Appendix 1

Equations of the Net CO$_2$ Assimilation Submodel

$$A_n = V_c\left(1 - \frac{\Gamma}{C_C}\right) - R_d \quad \text{Net CO}_2\text{assimilation rate} \tag{A1}$$

$$V_c = min\left(W_c, W_j, W_P\right) \qquad \text{Carboxylation rate} \tag{A2}$$

$$W_c = \frac{C_c V_{cmax}}{C_c + K_c\left(1 + \frac{O}{K_o}\right)} \quad \text{Rubisco} - \text{limited carboxylation rate} \tag{A3}$$

$$W_j = \frac{J}{4 + 8\frac{\Gamma}{C_c}} \quad \text{RuBP regeneration} - \text{limited carboxylation rate} \tag{A4}$$

$$W_P = \frac{3\ \text{TPU}}{\left(1 - \frac{\Gamma}{C_c}\right)} \quad \text{TPU} - \text{limited carboxylation rate} \tag{A5}$$

$$J = \frac{\alpha\ \text{PPFD}}{\sqrt{1 + \frac{\alpha^2 \quad \text{PPFD}^2}{J_{max}^2}}} \quad \text{Electron transport rate} \tag{A6}$$

$$P = exp\left(c - \frac{\Delta H_a}{R\left(T_{leaf}\right)}\right) \quad \text{Arrhenius temperature} - \text{response function for}\,\Gamma,\ K_C\ and\ K_O \tag{A7}$$

$$P = P^{25}\frac{exp\left(c - \frac{\Delta H_a}{R\ T_{leaf}}\right)}{1 + exp\left(\frac{\Delta S\ T_{leaf} - \Delta H_d}{R\ T_{leaf}}\right)} \quad \text{Arrhenius temperature} - \text{response function for}\,V_{cmax},\ J_{max},\ TPU\,\text{and}\,R_d \tag{A8}$$

Appendix 2

Empirical Photoinhibition Model

$$\Delta H_d = \Delta H_{d,max} - max\Big(0, \left(\Delta H_{d,max} - \Delta H_{d,T}\right) * min\left(1, \frac{\Psi_{leaf} - \Psi_{leafmax}}{\Psi_{leafmin} - \Psi_{leafmax}}\right)\Big) \tag{A9}$$

$$\Delta H_{d,T} = \Delta H_{d,T1} - \left(\Delta H_{d,T1} - \Delta H_{d,T2}\right) * min\left(1, max\left(0, \frac{T_{leaf} - T_{leaf1}}{T_{leaf2} - T_{leaf1}}\right)\right) \tag{A10}$$

where $\Delta H_d \left[\mathrm{kJ\quad mol_{CO_2}}^{-1}\right]$ is calculated after accounting for the joint effects of leaf water potential Ψ_{leaf} [MPa] and temperature T_{leaf} [K]; $\Delta H_{d,max} \left[\mathrm{kJ\quad mol_{CO_2}}^{-1}\right]$ is the value of ΔH_d without accounting for photoinhibition; $\Delta H_{d,T} \left[\mathrm{kJ\quad mol_{CO_2}}^{-1}\right]$ is the value of ΔH_d after accounting for the effect of T_{leaf}; $\Psi_{leaf,max}$ and $\Psi_{leaf,min}$ [MPa] are leaf water potential values at which photoinhibition starts and reaches its maximum effect, respectively; finally, $\Delta H_{d,T1}$ and $\Delta H_{d,T2} \left[\mathrm{kJ\quad mol_{CO_2}}^{-1}\right]$ are empirical thresholds corresponding to leaf temperatures T_{leaf1} and T_{leaf2} which are temperatures at which photoinhibition starts and reaches its maximum effect, respectively.

Appendix 3

Numerical Resolution

Initialization

1. Photosynthetic capacity parameters of individual leaves are calculated based on PPFD_{10} values using equations (9–11).
2. Leaf temperature (T_i) is assumed equal to that of the previous time step or equal to air temperature (T_{air}) for the first time step.
3. Collar water potential Ψ_{collar} is forced equal to soil water potential Ψ_{soil} as lower boundary of the hydraulic structure (only if the option of hydraulic structure is considered).
4. Xylem maximum and actual hydraulic conductivities of each internode (respectively $K_{max,i}$ and K_i) are calculated using, respectively, equations (2) and (3).
5. Xylem water potential at each node ($\Psi_{u,i}$) is assumed equal to that of the previous time step, otherwise, it is calculated using equation (1), assuming maximum hydraulic conductivities in all plant segments and considering the plant to be in hydrostatic equilibrium with the soil.

Convergence

When equation (1) is applied to a plant shoot of N segments, thus consisting of N nodes according to the graph theory, a system of N equations for $N + 1$ water head values is obtained. To solve the system for water potentials at all nodes, boundary conditions are set as follows: the lower boundary condition is a Dirichlet-type whereby a constant soil water potential value (Ψ_{soil}) is forced during each iteration; the upper boundary condition is a Neumann-type, whereby a constant flow (F_i) is forced at each leaf node (F_i is equal to transpiration E multiplied by leaf surface, cf. equation (6)). The calculation procedure is detailed in the numerical resolution section.

1. Leaf-scale A_n and E rates are calculated using equations (A1–A8) and (4–8).
2. E is multiplied by leaf surface area to obtain xylem flux (F_i) at the leaf-level, that is forced to the hydraulic structure system.
3. F_i values are calculated for each internode by 'walking downwards' from leaves to collar (post-order traversal on MTG).
4. New values of $\Psi_{u,i}$ are calculated from equation (1), assuming constant K_i, by 'walking upwards' (pre-order traversal on MTG) starting from the collar (where Ψ_{collar} is known) up to the leaves.
5. K_i values are updated using equation (2).
6. Steps 4 and 5 are repeated until convergence, that is the absolute difference ($\Delta\Psi_{u,i}$) between two consecutive iterations (respectively $j - 1$ and j) of at most one node, is lower than a predefined error threshold (ε_x):

$$\Delta\Psi_{u,i} = \left|\Psi_{u,i}^{j} - \Psi_{u,i}^{j-1}\right| \leq \varepsilon_x \tag{A11}$$

7. New T_i values are calculated from energy balance, considering the new E values in equation (14) using the following steps:
    a. In a first step, the surrounding temperature (T_{leaves}) is fixed at the first iteration (equal to T_{leaves} from the previous calculation step) and T_i is solved for each leaf.
    b. In a second step, T_{leaves} is updated considering the new values of leaf temperature and a new set of T_i values is computed.
    c. The first and second steps are repeated until the maximum absolute difference of the temperature of each leaf between two consecutive iterations falls below 0.02 °C (Maes and Steppe 2012).
8. Steps 1–7 are repeated until convergence, that is the absolute difference (ΔT_i) between two consecutive iterations (respectively $j - 1$ and j) of at most one leaf, is lower than a predefined error threshold (ε_T):

$$\Delta T_{leaf,i} = \left|T_{leaf,i}^{j} - T_{leaf,i}^{j-1}\right| \leq \varepsilon_T \tag{A12}$$

Appendix 4

Table A1. Table of variable symbols, values and units used for CO_2 net assimilation, stomatal conductance and hydraulic structure submodels. Values that are not referenced are obtained by using a *one-factor-at-a-time* method to minimize errors between simulated and observed data obtained at the grapevine experimental plot at the National Institute for Agricultural Research (INRA) in Montpellier (3°53′′E, 43°37′′N, 44 m alt).

Symbol	Value	Unit	Description
Energy balance			
α_{R_g}	0.6 [a]	–	Lumped leaf absorptance in the shortwave band
ε_{leaf}	0.96 [a]	–	Emissivity/absorptivity of the leaf in the thermal infrared (TIR) band
ε_{sky}	1 [a]	–	Emissivity/absorptivity of the sky in the TIR waveband
ε_{soil}	0.95 [a]	–	Emissivity/absorptivity of the soil in the TIR waveband
ε_T	0.02 [b]	K	Maximum allowable error in leaf temperature estimation
λ	0.044	$W\ s\ mol^{-1}$	Latent heat for vapourization
σ	$5.7\ 10^{-8}$	$W\ m^{-2}\ K^{-4}$	Stefan–Boltzmann constant
Φ_{R_g}	–	$W\ m^{-2}$	Flux density of global irradiance
K_{air}	–	$W\ m^{-1}\ K^{-1}$	Thermal conductivity of air
k_{sky}	–	–	Form factors of the sky
k_{soil}	–	–	Form factors of the soil
T_{sky}	–	K	Sky temperature
T_{soil}	–	K	Soil temperature
Hydraulic structure			
ϵ_x	0.05	MPa	Maximum allowable error in xylem water potential estimation
Θ_{soil}	–	–	Soil volumetric water content
ρ	0.98	$kg\ m^{-3}$	Water density
$\Psi_{crit,leaf}$	–0.65	MPa	Ψ_{leaf} that reduces PPFD to 50% of its maximum value
$\Psi_{crit,stem}$	–0.76 [c]	MPa	Shape factor regulating the steepness of the reduction in K due to cavitation
Ψ	–	MPa	Mean water potential of a hydraulic segment
Ψ_l	–	MPa	Water potential at the downstream limit of a hydraulic segment
Ψ_{leaf}	–	MPa	Leaf bulk water potential
Ψ_{soil}	–	MPa	Soil bulk water potential
Ψ_u	–	MPa	Water potential at the upstream limit of a hydraulic segment
c_{x1}	1.0	–	Shape factor regulating the effect of cavitation on xylem conductivity
c_{x2}	1.6 [d]	–	Shape factor regulating the relationship between K_{max} and D
c_{x3}	2.0 [d]	–	Shape factor regulating the relationship between K_{max} and D
D	–	m	Average diameter of a hydraulic segment
g	9.81	$m\ s^{-2}$	Gravitational acceleration
H_l	–	MPa	Water head at the downstream limit of a hydraulic segment
H_u	–	MPa	Water head at the upstream limit of a hydraulic segment
F	–	$kg\ s^{-1}$	Water flow across a hydraulic segment
K	–	$kg\ s^{-1}\ m\ MPa^{-1}$	Hydraulic conductivity of a hydraulic segment

Table A1. *Continued*

Symbol	Value	Unit	Description
K_{max}	–	$kg\ s^{-1}\ m\ MPa^{-1}$	Maximum conductivity of a hydraulic segment
L	–	m	Length of a hydraulic segment
z_l	–	m	Elevation of the downstream limit of a hydraulic segment
z_u	–	m	Elevation of the upstream limit of a hydraulic segment
Gas exchange			
α	0.2 [e]	$\mu mol_{CO_2}\ \mu mol_{photon}^{-1}$	Initial quantum yield
ΔH_a	–	$kJ\ \ {mol_{CO_2}}^{-1}$	Activation energy of the Arrhenius functions
ΔH_d	–	$kJ\ \ {mol_{CO_2}}^{-1}$	Deactivation energy of the Arrhenius functions accounting for photoinhibition
$\Delta H_{d,max}$	200 [e]	$kJ\ \ {mol_{CO_2}}^{-1}$	Deactivation energy in the absence of photoinhibition
$\Delta H_{d,T}$	–	$kJ\ \ {mol_{CO_2}}^{-1}$	Deactivation energy accounting for the effect of leaf temperature
$\Delta H_{d,T1}$	195	$kJ\ \ {mol_{CO_2}}^{-1}$	Deactivation energy at which photoinhibition starts
$\Delta H_{d,T2}$	180	$kJ\ \ {mol_{CO_2}}^{-1}$	Deactivation energy at which photoinhibition is maximum
ΔS	0.635 [e]	$kJ\ \ K^{-1}\ {mol_{CO_2}}^{-1}$	Entropy term
Δx	–	m	Thickness of the boundary layer
Γ	–	$\mu mol_{CO_2}\ \ {mol_{CO_2}}^{-1}$	CO_2 compensation point in the absence of mitochondrial respiration
v	–	$m\ s^{-1}$	Wind speed of ambient air
$\Psi_{leaf,max}$	–0.76	MPa	Leaf bulk water potential at which photoinhibition starts
$\Psi_{leaf,min}$	–2.00	MPa	Leaf bulk water potential at which photoinhibition is maximum
A_n	–	$\mu mol_{CO_2}\ \ m^{-2}\ s^{-1}$	Net CO_2 assimilation rate at the leaf scale
$A_{n,plant}$	–	$\mu mol_{CO_2}\ \ s^{-1}$	Net CO_2 assimilation rate at the plant scale
a_N	–0.0008 [e]	$g_N\ \ {g_{drymatter}}^{-1}\ {}^{\circ}Cd^{-1}$	Slope of the relationship between N_m and the cumulative degree-days temperature
a_M	6.471 [e]	$g_{drymatter}\ \ {mol_{photon}}^{-1}d$	Slope of the relationship between LMA and $PPFD_{10}$
b_{N_a}	–	$\mu\ mol_{CO_2}\ \ m^{-2}\ s^{-1}$	Intercept of the relationship between N_a and P^{25}
b_N	3.3 [e]	$g_N\ \ {g_{drymatter}}^{-1}$	Intercept of the relationship between N_m and the cumulative degree-days temperature
b_M	56.635 [e]	$g_{drymatter}\ \ m^{-2}$	Intercept of the relationship between LMA and $PPFD_{10}$
c	–	–	Shape parameter of the Arrhenius functions
C_i	–	$\mu mol_{CO_2}\ \ mol^{-1}$	Intercellular CO_2 concentration
D_0	1 or 30	$[kp_a]$	Scaling factor relating g to VPD
D_{H_2O}	$2.13{*}10^{-5}$	$m^2\ s^{-1}$	Diffusion coefficient of H_2O in the air at 0 °C
E	–	$mol_{H_2O}\ \ m^{-2}\ s^{-1}$	Transpiration rate per unit leaf surface area
E_{plant}	–	$mol_{H_2O}\ \ s^{-1}$	Transpiration rate of the entire plant
f_w	–	–	Stomatal sensibility to water stress function
g_{b,CO_2}	–	$mol_{CO_2}\ \ m^{-2}\ s^{-1}$	Boundary layer conductance to CO_2
g_{b,H_2O}	–	$mmol_{H_2O}\ \ m^{-2}\ s^{-1}$	Boundary layer conductance to water vapour
g_{s,CO_2}	–	$mol_{CO_2}\ \ m^{-2}\ s^{-1}$	Stomatal conductance to CO_2
g_{s,H_2O}	–	$mmol_{H_2O}\ \ m^{-2}\ s^{-1}$	Stomatal conductance to water vapour

Table A1. *Continued*

Symbol	Value	Unit	Description
g_{s0,CO_2}	0.02[e]	$\mathrm{mol_{CO_2}\ m^{-2}\ s^{-1}}$	Residual stomatal conductances to CO_2
g_m	0.1025	$\mathrm{mol_{CO_2}\ m^{-2}\ s^{-1}}$	Chloroplast conductance to CO_2
J	–	$\mathrm{\mu mol_{electron}\ m^{-2}\ s^{-1}}$	Electron transport rate
J_{max}	143.0[e]	$\mathrm{\mu mol_{electron}\ m^{-2}\ s^{-1}}$	Maximum electron transport rate
K_c	404.9[e]	$\mathrm{\mu mol\ mol^{-1}}$	Michaelis–Menten constant for the carboxylase
K_o	278.4[e]	$\mathrm{\mu mol\ mol^{-1}}$	Michaelis–Menten constant for the oxygenase
l	–	m	Mean length of the leaf blade in the downwind direction
m_0	5.7[e]	–	Scaling factor relating m_0 to A_n
n	4	–	Shape parameter regulating the water stress sensibility function of VPD, *kPa*
N_a	–	$\mathrm{g_N\ m^{-2}}$	Nitrogen content per leaf surface area
N_m	–	$\mathrm{g_N\ g_{drymatter}{}^{-1}}$	Nitrogen content per leaf dry matter
O	210[e]	$\mathrm{mmol_{O_2}\ mol^{-1}}$	Oxygen concentration
P	–	–	Value of any of Γ, K_c, K_o, V_{cmax}, J_{max}, TPU, R_d at actual leaf temperature T_{leaf}
P_a	0.101	MPa	Ambient air pressure at 0 °C
P^{25}	–	$\mathrm{\mu mol_{CO_2}\ m^{-2}\ s^{-1}}$	Value of any of V_{cmax}, J_{max}, TPU, R_d at leaf temperature T_{leaf} of 25 °C
PPFD	–	$\mathrm{\mu mol_{photons}\ m^{-2}\ s^{-1}}$	Photosynthetic photon flux density
PPFD_{10}	–	$\mathrm{\mu mol_{photons}\ m^{-2}\ s^{-1}}$	Leaf's cumulated irradiance averaged over the past 10 days
R	$8.315\ 10^{-3}$	$\mathrm{kJ\ K^{-1}\ mol^{-1}}$	Ideal gas constant
R_d	–	$\mathrm{\mu mol_{CO_2}\ m^{-2}\ s^{-1}}$	Mitochondrial respiration rate in the light
s_{N_a}		$\mathrm{\mu mol_{CO_2}\ g_N{}^{-1}\ s^{-1}}$	Slope of the relationship between N_a and P^{25}
T_{air}	–	K	Air temperature
T_b	283	K	Base temperature
T_{leaf}	–	K	Leaf temperature
T_{leaf1}	305	K	Leaf temperature at which photoinhibition starts
T_{leaf2}	306	K	Leaf temperature at which photoinhibition is maximum
TPU	–	$\mathrm{\mu mol_{CO_2}\ m^{-2}\ s^{-1}}$	Triose phosphate transport rate
V_c	–	$\mathrm{\mu mol_{CO_2}\ m^{-2}\ s^{-1}}$	Carboxylation rate
V_{cmax}	89.0[e]	$\mathrm{\mu mol_{CO_2}\ m^{-2}\ s^{-1}}$	Maximum carboxylation rate
VPD	–	kPa	Vapour pressure deficit
W_c	–	$\mathrm{\mu mol_{CO_2}\ m^{-2}\ s^{-1}}$	Rubisco-limited carboxylation rate
W_J	–	$\mathrm{\mu mol_{CO_2}\ m^{-2}\ s^{-1}}$	RuBP-limited carboxylation rate
W_p	–	$\mathrm{\mu mol_{CO_2}\ m^{-2}\ s^{-1}}$	Triose phosphates-limited carboxylation rate

[a] Nobel (2005).

[b] Maes and Steppe (2012).

[c] Jacobsen *et al.* (2015).

[d] Tyree and Zimmermann (2002).

[e] Prieto *et al.* (2012).